

**Scrape Off Layer turbulence and flow velocity measurements
with the Li-beam diagnostic**

Jorge Rodriguez Serra

Supervised by:

Prof. Dr. S. Zoletnik

Prof. Dr. Alfredo de Blas

ETSEIB

Departament d'Energia Nuclear



Scrape Off Layer turbulence and flow velocity measurements with the Li-beam diagnostic

Jorge Rodriguez Serra

September 26, 2016

Abstract

En aquest treball s'estudien els fluxes i turbulències generats a l'interior d'un reactor nuclear. Un dels grans problemes que afronta ara la implementació de la fusió nuclear és el control i rendiment de la reacció, cosa que ve molt afectada pel comportament de fluxes interns i les turbulències que s'hi generen.

D'aquesta manera, s'estudien, concretament, l'existència i el comportament de les turbulències i el comportament i la velocitat del flux que apareixen a la capa externa del plasma dins del reactor.

Aquest estudi es fa analitzant i filtrant dades obtingudes del reactor experimental Tokamak ASDEX Upgrade, situat a les afores de Munich, Alemanya. L'experiment d'on es treuen les dades consisteix en fer entrar un feix col·limat de partícules accelerades de liti a dins del reactor. Aquestes partícules reaccionen amb les partícules del plasma i emeten fotons, que són captats pels sensors òptics del reactor. Les dades obtingudes són tractades primerament amb transformacions matemàtiques, començant per fent la transformada de Fourier per a poder canviar del domini temporal al domini freqüencial, i així aconseguir l'espectre de potència. i després graficades per a poder treure conclusions sobre el comportament del fluxe del plasma a dins d'un reactor de fusió nuclear.

S'aprofita aquest treball també per a guanyar coneixement en la fusió nuclear i en els reactors on s'hi dona, i és per això que es fa èmfasi en estudiar el seu funcionament.

Finalment s'evalua l'impacte mediambiental i econòmic del projecte.

—

Acknowledgements

This work would not have been possible without the academic and moral support of many people.

First I'd like to thank Dr Sandor Zoletnik, my tutor during this research, for all his knowledge and always ready to help with a book or a meeting. Also, I have a deep gratitude with professor Alfredo de Blas del Hoyo, who had an enormous patience and have been very supportive when needed. A special thank to my family and friends for his enormous support during these years of degree. I want to finish thanking my girlfriend Julia. She has been the most supportive and helpful person in the last year and she always tries to cheer me up. Thanks a lot for these moments.

Contents

1	Preface	8
2	Introduction	9
2.1	Research motivation	9
2.2	Research focus	12
2.3	Research goal	13
2.4	Thesis outline	13
3	Theoretical frame	15
3.1	Nuclear fusion	15
3.1.1	Lawson Criterion	17
3.1.2	Geometry and plasma confinement	18
4	Materials and methods	26
4.1	ASDEX Upgrade	26
4.2	Diagnosis methods	27
4.2.1	Lithium beam	27
4.3	Experiment setup	29
4.3.1	Selection of time intervals	30
4.4	Data treatment	31
4.4.1	Fourier transform	31
4.4.2	Calculating the power spectra	32
4.4.3	Estimation of noise level	33
4.4.4	Calculation of fluctuation amplitude	34
4.4.5	Calculation of correlations an flow velocity	34
4.5	Algorithm	35

5	Results and discussion	36
5.1	Fluctuation amplitude and flow velocity profiles	36
6	Ecological and economic analysis	49
6.1	Budget	49
6.1.1	Human resources	49
6.1.2	Material resources	50
6.1.3	Energetic resources	51
6.2	Ecological analysis	51
7	Conclusions	52
7.1	Findings	52
7.2	Goals achievement	53
7.3	Future work	53
	Appendices	57
A	Used code	58
A.1	Main code	58

List of Figures

3.1	Two nuclei, deuterium and tritium, fuse and form a helium nucleus, a neutron and energy [1]	16
3.2	Nuclear binding energy	17
3.3	Chemical structure of deuterium and tritium, where the white balloons represent neutrons attached to the nucleus [2]	18
3.4	Lawson criteria depending on Lawson's triple product [3] for three different reactions [4].	19
3.5	Dependence of the burn fraction on the ρr parameter for uniformly heated sphere for different temperatures	21
3.6	Behavior of a charged particle under a magnetic field.	23
3.7	Representation of the separatrix and the SOL in a toroidal device [Institut für Plasmaforschung]	24
3.8	Tokamak's magnetic system [Bar 96]	25
3.9	Magnet coils and plasma (yellow) of a stellarator [5]	25
4.1	The improve version of the ASDEX gun, source: [6]	28
4.2	raw signal obtained from ASDEX Up	29
4.3	Plasma heating current of discharge 30545	29
4.4	The selection of the time intervals seen on the raw signal from the divertor, density 1.	30
4.5	The selection of the time intervals seen on the raw signal from the divertor, density 2.	31
4.6	Power spectra of the signals from all the channels on shoot 30548	33
4.7	Power spectra of the intended signal, noise and the obtained signal	34
5.1	Plasma profile during 30545 experiment. Source: IPP	37

5.2	Relative fluctuation amplitude and poloidal velocity in shot 30545 during L mode with density 1.	38
5.3	Relative fluctuation amplitude and poloidal velocity in shot 30545 during the first part of the intermediate phase with density 1. . .	38
5.4	Relative fluctuation amplitude and poloidal velocity in shot 30545 during the second part of the intermediate phase with density 1. .	39
5.5	Relative fluctuation amplitude and poloidal velocity in shot 30545 during H mode taking the data in between ELMs with density 1.	39
5.6	Relative fluctuation amplitude and poloidal velocity in shot 30545 during H mode during the ELMs, with density 1.	40
5.7	Relative fluctuation amplitude and poloidal velocity in shot 30545 during the L mode with density 2.	40
5.8	Relative fluctuation amplitude and poloidal velocity in shot 30545 during the first part of the intermediate phase with density 2. . .	41
5.9	Relative fluctuation amplitude and poloidal velocity in shot 30545 during the second part of the intermediate phase with density 2. .	41
5.10	Relative fluctuation amplitude and poloidal velocity in shot 30545 during the H mode, taking the data between the ELMs. With density 2.	42
5.11	Relative fluctuation amplitude and poloidal velocity in shot 30533 during L mode with density 1	42
5.12	Relative fluctuation amplitude and poloidal velocity in shot 30533 during the intermediate phase with density 1	43
5.13	Relative fluctuation amplitude and poloidal velocity in shot 30533 during H mode and density 1.	43
5.14	Relative fluctuation amplitude and poloidal velocity in shot 30533 during the L mode with density 2.	44
5.15	Relative fluctuation amplitude and poloidal velocity in shot 30533 during the intermediate phase with density 2.	44
5.16	Relative fluctuation amplitude and poloidal velocity in shot 30533 during the H mode and taking only the data between the ELMs, with density 2.	45

5.17	Relative fluctuation amplitude and poloidal velocity in shot 30533 during the H mode and taking only the data during the ELMs, with density 2.	45
5.18	Relative fluctuation amplitude and poloidal velocity in shot 30534 during H mode between ELMs and density 1.	46
5.19	Relative fluctuation amplitude and poloidal velocity in shot 30534 during the L mode with density 2.	46
5.20	Relative fluctuation amplitude and poloidal velocity in shot 30534 during the intermediate phase with density 2.	47
5.21	Relative fluctuation amplitude and poloidal velocity in shot 30534 during the H mode and taking only the data between the ELMs, with density 2.	47
5.22	Relative fluctuation amplitude and poloidal velocity in shot 30534 during the H mode and taking only the data during the ELMs, with density 2.	48

List of Tables

4.1	ASDEX Up characteristics	27
6.1	Human resources used on the creation of this thesis and their economic cost	49
6.2	Material resources used on the creation of this thesis and their economic impact	50

Chapter 1

Preface

During the period between October 2014 and may 2015 I carried out a research at the MTA Wigner Research Centre for Physics in Budapest, Hungary. With the guide of professor Sandor Zoletnik and his colleges Dániel Dunai and Gergő Pokol. The research was focused on the behavior of the scrape off layer of the thermonuclear experimental reactor ASDEX upgrade, located in Munich.

This thesis shows the results of this research.

Chapter 2

Introduction

This work studies the behavior of the plasma in the outer part of the vessel, where the magnetic field lines are no longer closed, this part is called scrape off layer. The machine studied is the experimental fusion reactor ASDEX upgrade. This chapter will introduce the topic of this research project. The motivation of the research is explained firstly, followed by research focus and research background. Finally, the thesis outline is given.

2.1 Research motivation

Humanity consumes the planet resources faster every day. As technology advances human need advance too and also the consumption of planet resources. According to the IEA (International Energy Agency) on June, 2013, fossil fuels were covering 80% of global energy demand [7]. Even with the commitment of every country to make changes to fight against global warming, even achieving other challenges in the direction of reducing consumption, the energy demand will increase globally by 40% before 2035 (with fossil fuels still covering 75%) [8]. And taking into account the planet reserves and current consumption rates we can assume the following:

- Oil is expected to last in the range of 40 to 45 years. However, this period may be increased as resources are successfully converted into reserves, as it happened before. Global reserves have increased since 1990 despite growth in consumption.

- Conventional gas is thought to remain in the range of 55 to 60 years. Nevertheless, unconventional gas reserves coming from hydraulic fracture are very difficult to be estimated, because of rock formation heterogeneity.
- Reserves of coal are bigger than other fossil fuels and the ratio is in between 110 and 120 years at current consumption ratio. Anyway, due to modern regulations to prevent major effects coming from pollution, the use of coal is being reduced.

With necessary resources of fossil fuels meeting the increasing energy demand, Resources to Reserves 2013 [8] shows that the emphasis should be on technology, prices and policies. To be able to ensure resources in financially viable and environmentally sustainable ways.

Fossil fuels have a great impact on environment, so nuclear energy appears to be a great alternative, since remarkable amounts of energy that can be obtained by this energy. Currently, nuclear fission, can be safely handled. Despite of this, the fuel extraction, enrichment, reprocessing and burning of heavy metals (like uranium), produce radioactive waste which can damage environment during very long periods of time. Despite of the high security, danger of possible accidents in fission power plants generate a big rejection from the population towards nuclear energy.

At this point, ecological and renewable energies are a great alternative. Towards the middle of the current century, the power supplied by renewable energies is expected to suffer a significant increase, sadly it is also expected to barely cover the growth of the global energy demand. Some studies have pointed out that the prices of electricity obtained from renewable sources will fall [9].

In the race for global energy supply we have, on the one hand, fossil fuels that can ensure supply for a limited time of some decades while increasing pollution and global warming. And on the other hand, renewable energies that represent an unlimited and ecological resource of energy, but incapable to cover the increasing energy demand. Hence, the need to find a new and powerful enough energy source able to fulfil the system demands and to do it in a sustainable way. Requirements met by nuclear fusion. Therefore the importance of achieve the challenge of controlling it.

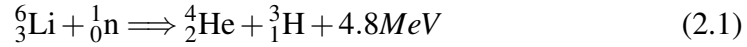
Fusion is the energy from the stars. Sir Arthur Eddington proposed, in 1926, that there is a limit where the pressure of the stars light on the atmosphere is

large enough to balance the gravitational weight of the stellar atmosphere entirely, known as the Eddington luminosity limit [10]. If a star was any brighter, light would eliminate the outer layers of the atmosphere and cause the star to lose mass. The physicist defined stars as gas spheres at very high temperature, basically made of hydrogen [11]. The pressure of gravitational forces can reach a temperature that turns gases into plasma (the fourth state of the matter). In 1927, Dr. Lewi Tonks and Dr. Irving Langmuir defined plasma as an almost neutral ionised gas where electrons and ions are moving independently [12]. The pressure and temperature in the stars get hydrogen nuclei to fuse in plasma producing helium and gaining energy. Therefore, nuclear fusion tries to generate electricity reproducing the reaction happening in the stars. The fuel used in nuclear fusion reactors is tritium (a hydrogen radioactive isotope, which can be taken from lithium, see figure 3.1). It is important to remark the low CO_2 emissions (6 - 12 Cg/kWh) of nuclear fusion, followed by hydroelectric energy (4.8 Cg/kWh) and light water reactors (5.7 Cg/kWh). Photo-voltaic (16 Cg/kWh) and Wind (33.7 Cg/kWh) energy productions have low CO_2 emissions too but the contra is the production processes and the unstable production of energy. This is to say, they are not able to produce reliable continuous power. However, oil (200 Cg/kWh) and coal (270 Cg/kWh) are the most contaminant energies [13].

There are two great advantages in fusion against fission. First, and in contrast to fission, which employs a large quantity of uranium or plutonium fuel, nuclear fusion employs a very small amount of tritium and deuterium fuel. If fuel is not continually replaced, the fusion reaction goes out and stays out, so there is no danger of an accident. Nuclear fusion is a reaction happened in stars, not in the Earth.

The second advantage is the low radioactive waste. Radioactive materials resulting from the fission fuel cycle, need to be separated from the unburned fuel and safely stored for thousands of years. This process is extremely difficult and expensive and not absent of danger. Nuclear fusion generates almost none radioactive waste, the resulting of the fusion reaction is helium gas and tritium. It is true that tritium is a radioactive element but decays much faster (12.32 years half-life) than uranium (238.45 million years half-life), and when the technology will be developed, the purpose is to recycle the tritium used in the fusion power-plant. In addition, there is no need of aggressive mining exploitation since deuterium

and tritium have to be obtained from other sources. Oceans have a small proportion of deuterium in their waters and tritium is obtained from a lithium nuclear reaction, see figure 2.1. There's enough lithium on earth to last for ten thousands years and enough deuterium in the oceans [14].



On the other hand we have to be aware, in fusion power, of the possibility of a tritium fallout that would cause a severe environmental problem. And also the fact that the reactor walls, due to the neutrons interaction, will remain activated for several decades [15] once the useful life is over.

Since the discovery of the fusion reaction in the 1930s humanity has been trying to control this reaction in order to obtain energy from it without much success. It represents a technological and physic challenge yet to solve. There are many obstacles in the way towards a useful fusion reactor: the needed temperature of 150 million degrees Celsius [16], the confinement of the plasma within the vessel, the losses of heat, etcetera.

2.2 Research focus

This research focuses in the needs of understanding the behavior of the plasma in the outer layers of the vessel. While the charged particles inside the plasma are controlled by the presence of a strong magnetic field, this forces lose strength when the field is interrupted by the presence of some solid element. The space this last closed flux surface (LCFS) and the wall of the vessel is called Scrape Off Layer (SOL). At this point the magnetic field cannot hold the plasma in a regular way, this causes turbulence' in the plasma that needs to be investigated in its own manner.

We know that the heat transport in the SOL is determined by plasma turbulence and, that's why measuring the scrape off layer is important, since it is in this layer where energy and the particles are flowing and where the energy can be collected through the walls.

In this work, we have studied the behaviour of the turbulence's created in the scrape off layer, with data from the ASDEX Upgrade, located in Germany.

2.3 Research goal

The goal of this research is to design and implement a program to calculate the dimension of the turbulence generated in the SOL and how they behave. Firstly the existence and magnitude of the turbulence is studied and, secondly, the transport inside the the reactor of those turbulence is studied as well at both sides of the LCFS.

The data used comes from a plasma discharge and we assume that the behavior the tho studied turbulence will be the same during a fusion reaction. Therefore, the main goal of this thesis is to throw some light and give some hints on how turbulence behave inside the SOL to be able in the future to predict and control the heat transport to the walls.

The main question this thesis aims to answer is: How turbulence generated in the SOL behave?

The following sub questions are derived from the main question:

- What is a typical setup for a fusion reactor? And for ASDEX Upgrade in particular?
- What is a possible design for the program to filter data in order to see how turbulence behave?
- What is the dimension and importance of these turbulence in the fusion reaction?

To sum up, the goal of this work is to reach a better understanding of the behavior of the turbulence's in the SOL, as well as getting a broad knowledge on nuclear fusion and nuclear reactors.

2.4 Thesis outline

This thesis is organized as follows:

- In Chapter 2, the theoretical frame is explained. We give a brief introduction on the concepts of nuclear fusion, plasma and the conditions to achieve the fusion. Finally, we get deeper into closed confinement systems and explain two types of reactos: the tokamaks, and the stellarators.

- In Chapter 3, materials and methods are introduced. Firstly, we present the reactor whose datae has been studied. Then, we explain the diagnosis method used and the experiment setup. Finally, we give an explanation on how the data is treated.
- In Chapter 4, the results are shown and some discussion is made on them.
- In Chapter 5, the excological and economic analysis of this project is performed, giving some numbers on the sustainability of it.
- Finally, in Chapter 6, some conclusions are drawn and some hints of future work are thrown.

Chapter 3

Theoretical frame

In this chapter, a broad review of the theoretical frame is performed. Starting with a basic explanation .

3.1 Nuclear fusion

Nuclear fusion is a reaction in which the nuclei of two light atoms, unite to form a heavier nucleus. Usually, this union is followed by some other particle emission in order for the new atom to gain stability. For example, in the case of uniting a deuterium and a tritium, a neutron is emitted (see figure 3.1). The nuclear fusion reaction in light atoms causes a mass defect which, according to Einstein's formula $E = mc^2$, can release a great amount of energy in the form of kinetic energy from the emitted particles.

The binding energy of the neutrons and protons is maximum around iron. Therefore, fusion releases energy when the resulting nucleus is lighter than iron in order to obtain energy from the reaction, as can be seen in image 3.2.

The approach and fusion between two particles need high energy due to the Coulomb repulsion forces. Therefore, atoms need to be highly energetic and need to have thermal energy enough to fuse. In the sun, due to huge pressure caused by gravity it happens with a temperature of a few million degrees [17], with low pressure nuclei fuse around 100 million °C, what is well above the binding energy of the electrons. Thus, the atoms will loose their electrons. The mass formed by free electrons and ions is called plasma.

The fuel used in a thermonuclear reactor is, mainly, deuterium and tritium,

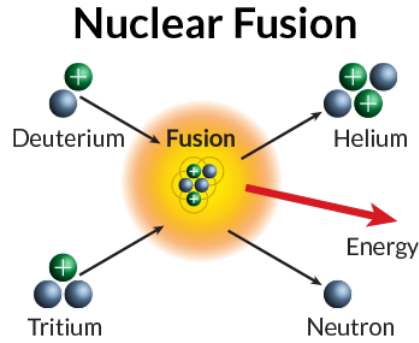


Figure 3.1: Two nuclei, deuterium and tritium, fuse and form a helium nucleus, a neutron and energy [1]

which are both isotopes of hydrogen (see figure 3.3). Deuterium is a stable isotope formed by a proton and a neutron. Its natural abundance in ocean water is about one atom for 6420 hydrogen. This means that the seawater has a concentration of 34 grams of deuterium per cubic meter of water. Deuterium energy content is so high that the power obtainable from deuterium in a liter of seawater is equivalent to the energy that can be obtained from 250 liters of burned oil [13]. Therefore, given that three quarters of the planet is covered by water, nuclear fusion is considered as an inexhaustible source of energy.

The other element used in nuclear fusion, tritium, is unstable so it cannot be found on the nature. It is composed of one proton and two neutrons and it disappears by beta emission decay relatively quickly. Tritium can be generated by neutron capture reactions with lithium isotopes. Lithium is an abundant material in the Earth's crust and seawater and, therefore, easy to obtain.

Fusion reactions Every element has its own cross section to cause fusion but, on Earth, with the condition we have and with the aim of obtaining energy, we should use light elements in fusion reactions. The most used elements in those reactions are hydrogen and its isotopes: the Deuterium (D) and the tritium (T), as mentioned before. The most suitable reactions for a controlled production of

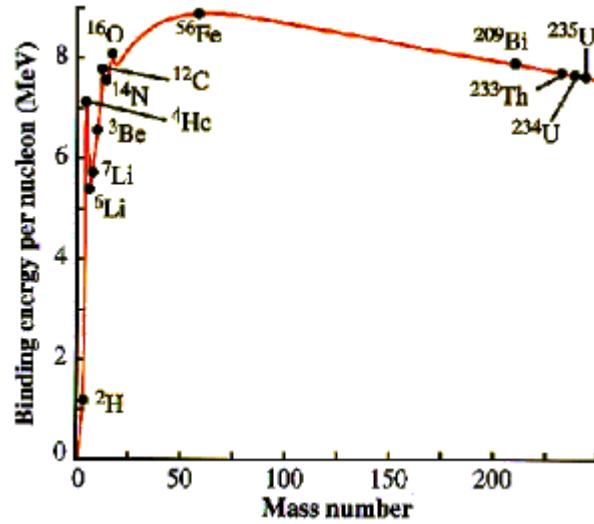
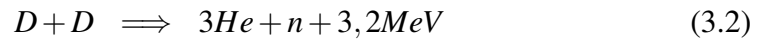
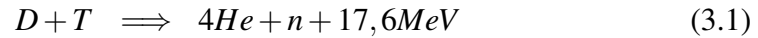


Figure 3.2: Nuclear binding energy

energy inside a reactor are:



Such reactions can only happen if the nuclei have enough kinetic energy.

The conditions to bring out fusion reactions are defined by the Lawson criteria, see subsection 3.1.1. The state of the matter where the fusion reaction happens is plasma and, therefore, it is on the plasma where the Lawson criteria needs to be fulfilled.

3.1.1 Lawson Criterion

If we perform an energy balance on the plasma using as physic parameter the density, temperature and confinement time, we will see that in order achieve an sustainable fusion reaction we need the plasma to have:

- with a high enough temperature T which may produce fusion
- a high density n to have enough particles to maintain the fusion reaction



Figure 3.3: Chemical structure of deuterium and tritium, where the white balloons represent neutrons attached to the nucleus [2]

- a confinement time τ_E long enough to obtain energy gain.

The energy gain (Q) is the proportion between fusion power produced by the thermonuclear reactor and the power needed to keep the plasma steady.

For every kind of fusion reaction there is a product τ_E which depends on the plasma temperature, it is called: "Lawson criterion"

For example, for a D-T fuel and a temperature of 10 keV (where $1\text{keV} = 1.6 \cdot 10^7\text{K}$) the product τ_E equals $10^{14} \text{ s} \cdot \text{cm}^3$ [18]. Which means that for a fusion plasma with magnetic confinement, whose density is in between 10^{14} and 10^{15} particles per cm^3 (ppcc), the confinement time is the order of magnitude of one second, but for a fusion plasma with inertial confinement, whose density is between 10^{25} and 10^{26} ppcc, that time would be 10^{-12} s (see figure 3.4)

3.1.2 Geometry and plasma confinement

The plasma where the fusion takes place is so hot that no material container could resist the extremely high temperatures. Hence, the need to find some alternative ways to confine the plasma in order to produce fusion. Two different methods are used to develop this task, magnetic confinement and inertial confinement.

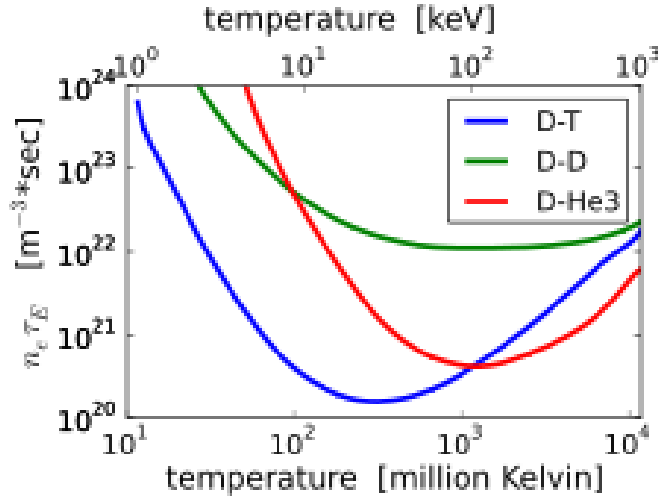


Figure 3.4: Lawson criteria depending on Lawson's triple product [3] for three different reactions [4].

Inertial confinement

At the derivation of the Lawson criterion we assumed that the system is stationary. The Hydrogen bomb showed that fusion energy production is possible in an explosion as well, therefore let us study the fusion energy balance of a freely expanding system. This is called inertial confinement as the material is confined by the finite expansion speed creating a medium so dense that rise greatly the probability of particle to collide. Let us assume that a sphere with material mix of 50% Deuterium and 50% Tritium is heated to fusion temperatures. This sphere of N nuclei will expand with c_S sound speed:

$$\rho = \frac{N}{4\pi r^3/3} \quad (3.4)$$

The density falls to half in time.

$$\tau = \frac{r_0}{c_S} \text{time} \quad (3.5)$$

The number of fusion reactions in the whole sphere in dt time is:

$$N_f = N_D n_T \langle \sigma v \rangle dt \quad (3.6)$$

During the whole expansion process the fraction of fused material (burn fraction) is:

$$f = \frac{1}{N_D} \int_0^\infty N_f dt = \langle \sigma v \rangle \cdot \int_0^\infty \frac{N/2}{4\pi(r_0 + c_s t)^3/3} dt \quad (3.7)$$

Which, simplified, results in the following equation.

$$f = \frac{\langle \sigma v \rangle}{2c_s} n_T^0 r_0 \quad (3.8)$$

Inserting the rate coefficient $\frac{\langle \sigma v \rangle}{c_s}$ of the D-T fusion reaction at 30 keV temperature we get:

$$f \sim \rho r_0 \quad (3.9)$$

where the density is in g/cm^3 and the radius is in cm. During the burn, fusion reduces the density of the DT nuclei and adiabatic expansion decreases temperature, which in turn reduces the fusion rate, thus our calculation is only approximate. Results on more detailed calculations are shown in figure 3.5. At 30 keV energy the curves approximate $f \approx \frac{\rho r}{6 + \rho r}$, where the density is in g/cm^3 and the radius is in cm. According to these calculations the maximum of the burn fraction is about 0.3 for $\rho r \simeq 1$. From this, we get that the fusion energy gain from the process is:

$$G_{max} \approx \frac{17.000keV \cdot 0.3}{2 \cdot 30keV} = 85 \quad (3.10)$$

As the thermal-electric conversion efficiency is around 30% and the heating system efficiency is also expected to be below 10% it seems unlikely that an inertial confinement fusion reactor can be built by heating the sphere uniformly.

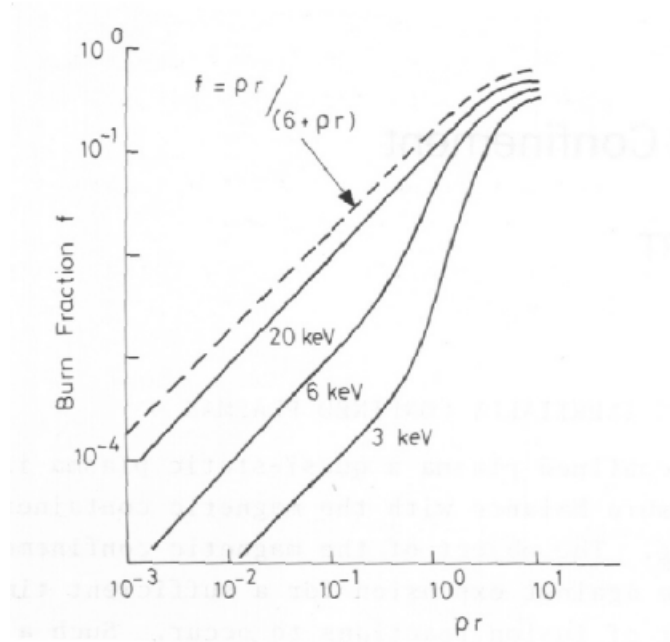


Figure 3.5: Dependence of the burn fraction on the ρr parameter for uniformly heated sphere for different temperatures

α heating also works in inertial fusion as the α particles can deposit their energy in the sphere by collisions. The number of collisions for an α particle while traveling out from the sphere is:

$$N_c = \sigma r \rho, \quad (3.11)$$

where, again, ρr is the determining parameter. This way α heating can induce a propagating burning wave if $\rho r > 0.3 \text{ g/cm}^2$

In case of propagating burn only a small $\rho r > 0.3 \text{ g/cm}^2$ part of the sphere needs to be heated to fusion temperatures which improves the energy balance. Additionally if $\rho r > 5 \text{ g/cm}^2$ then even neutrons can deposit their energy in the sphere which even more increases efficiency. We could see above that ρr has to be around 1 to build a fusion reactor. This could be achieved by e.g. $\rho = 1 \text{ g/cm}^3$; $r = 1 \text{ cm}$. However, from 1 g D-T mixture $3 \times 10^5 \text{ MJ}$ fusion energy is released, equivalent to 75 MT TNT explosion, same as a big nuclear bomb. This can obvi-

ously not be handled in a reactor, therefore we need to limit the energy production from one explosion

Magnetic confinement

Magnetic fields are ideal to confine plasma with high density, temperature and pressure during relatively long periods of time [19] Due to Lorentz forces. This force F comes from the interaction of the charged particles ions and electrons with the magnetic field they are in. This force makes the charged particle to follow an specific direction which keeps the away from the reactor walls.

Confinement consist on keeping material in plasma state inside a magnetic field with an specific shape or geometry. This is possible due to the interaction of the positives and negatives particles of the plasma with the magnetic field called Lorentz force. This force acts on the charged particles on a perpendicular direction to the magnetic field, which keeps them inside the geometry. The magnetic confinement is useful because it allows to heat matter until temperatures where no material container could keep its solid state. Unfortunately these method can keep low density plasma, around $10^{20} \text{ ions}/\text{m}^3$ [20]; but long confinement times, around 1 second [19]. In case of a hard break down the system would be considered as a failure due to his unavailability to create the required energy.

The following equation states that the acceleration of a particle within the plasma is perpendicular to both the velocity and the magnetic field, as shown in figure 3.6

$$\vec{F} = q\vec{E} + q\vec{v} \times \vec{B}, \quad (3.12)$$

All magnetic confinements relies on the same basic concept: charged particles, due to Lorentz force tend to move along magnetic field lines on Larmor precession, but two major types of geometries can be distinguished: open systems and closed systems depending on whether the field lines stay in the confinement region or not. In MCF (magnetic confinement fields), magnetic fields are used to

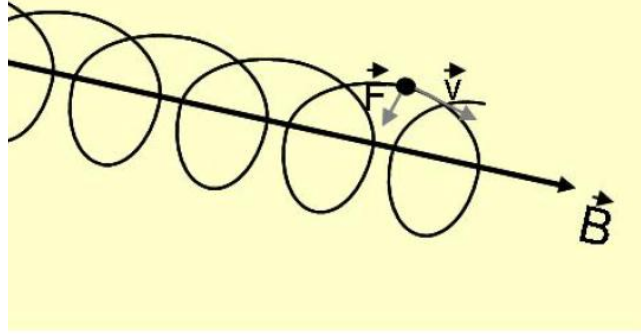


Figure 3.6: Behavior of a charged particle under a magnetic field.

confine plasma. Magnetic fields behave as though they have a pressure.

$$P_B = \frac{B^2}{2\mu_0} \quad (3.13)$$

Producing more than a few Tesla using magnets is difficult, so taking $B = 1\text{T}$ and a temperature $T = 10\text{keV}$ gives

$$n \approx 1.2 \cdot 10^{20} \text{m}^{-3} \quad (3.14)$$

Closed systems We define as close a confinement system where the magnetic field lines are closed. We have basically two different geometries used in closed field reactors: tokamak and stellarators. In this systems is where we have the Scrape Off Layer. The scrape off layer is the part of the plasma between the edge of the plasma, limited by the LCFS or the separatrix. In this zone magnetic field is not uniform and it is difficult to predict the behavior of the particles and heat transport. See figure 3.7.

Tokamaks

The term tokamak comes from the acronym toroidalnya kamera y magnetnaya katushka which means toroidal chamber and magnetic coil in russian. The magnetic field of a tokamak is created with coils placed around the torus (toroidal coils) while the poloidal magnetic field is created by an induced current I_p inside the plasma in the toroidal direction by a central solenoid. This current is induced by the poloidal coils which acts as the primary circuit of a transformer whose

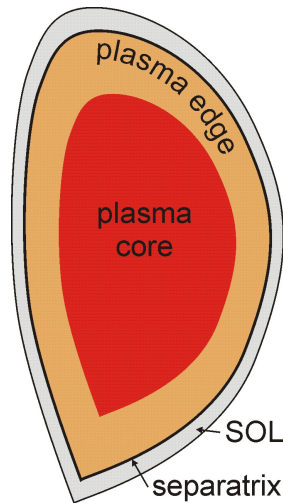


Figure 3.7: Representation of the separatrix and the SOL in a toroidal device [Institut für Plasmaforschung]

secondary circuit would be the plasma. The resulting field lines are the combination of those two fields (poloidal and toroidal), and have a helical shape along the torus. This shape allows particles to travel between inner and outer parts of the torus and holds the plasma in place.

Stellarators

Stellarators are also toroidal devices, but unlike the Tokamak, the magnetic poloidal field is not generated by an electric current along the plasma but only through exterior coils. The shape of these coils isn't yet standard and almost every stellarator device has different coil geometries. And since no current is induced in the plasma, stellarator devices can have a continuous performance and avoid disruption risks. The first magnetic confinement machine was based in this concept, but due to the complexity of its design there couldn't achieve the expected results and was slowly abandoned due to the good results of the first tokamaks. The problem was the low tolerance of the construction, the smallest deviation could cause a dysfunctional confinement, because all magnetic fields were created with complex geometry coils.

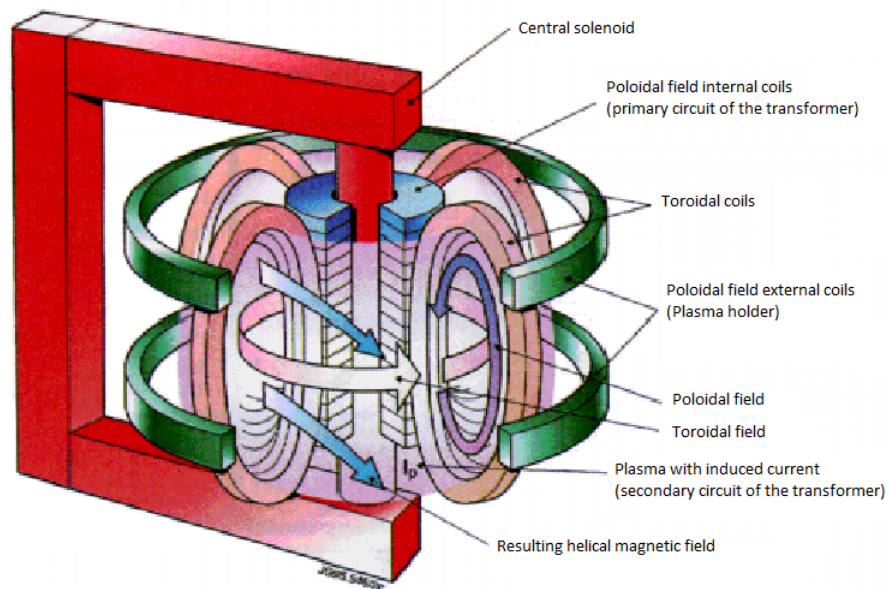


Figure 3.8: Tokamak's magnetic system [Bar 96]

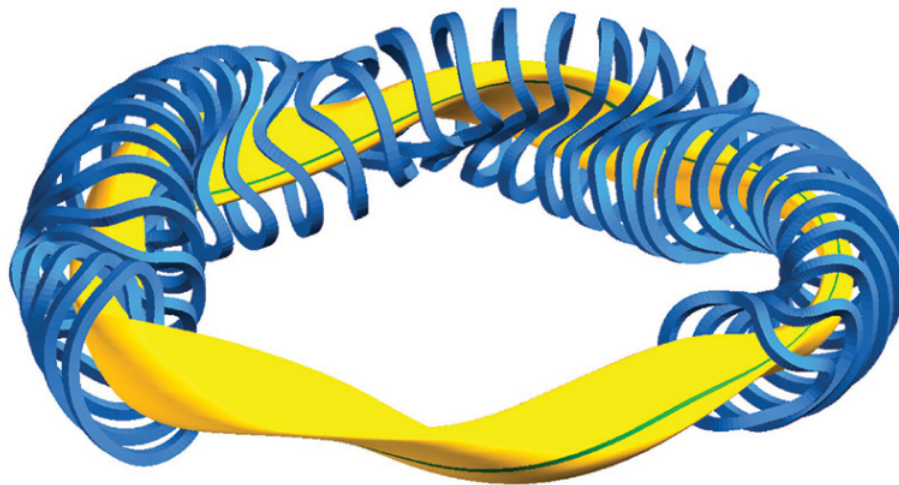


Figure 3.9: Magnet coils and plasma (yellow) of a stellarator [5]

Chapter 4

Materials and methods

In this chapter we will explain how the data was obtain and the methods used to analyze .

4.1 ASDEX Upgrade

All data used in this thesis comes from the tokamak reactor Axial Symetric Divertor Experiment Upgrade or ASDEX Upgrade. This machine is a medium sized (major radius $R = 1.65$ m, minor radius $r = 0.5$ m) tokamak experiment and is located in Garching, near Munich in Germany. It was designed to develop a reactor-compatible open divertor configuration, like ITER. In ASDEX, the parent tokamak of ASDEX Upgrade, the H-mode was observed for the first time . The divertor configuration enables a much easier access to H-mode. The goal of ASDEX Upgrade is to give physics input to critical elements of the ITER design and the preparation of ITER operation . It has an ITER like configuration with an elongated cross-section, flexible shaping capability. The heating system is versatile and has a total power of up to 27MW. Therefore, it is very suitable to study ITER relevant plasmas. In ASDEX Upgrade, the pedestal width amounts to about 1.5 cm . This makes the investigation and characterization of the pedestal very challenging. Furthermore, the transition to H-mode and other transient edge events take place on a sub-millisecond timescale. This requires edge diagnostics with a high temporal resolution.

Table 4.1: ASDEX Up characteristics

	Technical data:
Total height of the device	9 metres
Major plasma radius	1,6 metres
Minor plasma radii	0.5 - 0.8 metres
Magnetic field	3,9 tesla
Plasma current	2 megaamperes
Pulse length	10 seconds
Plasma heating	27 megawatts
Plasma volume	13 cubic metres
Plasma quantity	3 milligrams
Plasma mixture	hydrogen, deuterium
Plasma density	2×10^{20} particles per m^3
Plasma temperature	100 million degrees

4.2 Diagnosis methods

There are many methods that have been successfully tested and approved [21]. As mentioned before, the goal of this research is to throw some light on the turbulence created inside the fusion reactor, in the SOL. From all the possible diagnosis method there are two that are specially suitable for looking into turbulence in the outer parts of the plasma tanks to their accuracy, penetration and low contamination rate. Those methods are gas-puff imaging and beam emission spectroscopy [6, 19, 22], in our case, Li-beam spectroscopy

4.2.1 Lithium beam

The li-beam diagnosis consist on shooting fast neutral atom on lithium into the plasma and observing the light emitted during the interactions. The principle of the Li beam is the resonance radiation emitted from a neutral beam as it traverses the plasma. In the plasma, the lithium atoms are excited, this excitement decays emitting a photon with a characteristic wavelength ($\lambda = 670.8nm$). Observing the intensity of this radiation it is to deduce an electronic density profile $n_e(z)$ (being z the radius of the torus). The reconstruction technique is relatively simple for thermal beams, but more energetic beams demands complex models that consider electrons as well as excitation, ionisation and charge exchange in all the plasma

[23, 24], the model used to recreate the density profile was the one created by the Intitut für PlasmaPhysik (IPP) of the Max-plank institute [24]. The energy of the used beams is around 40-60keV, which provides 10-20 cm penetration into the plasma [19]. Higher energy would provide deeper penetration but the neutralisation of the beam would be compromised, and as see in figure 5.1 10 cm is enough.

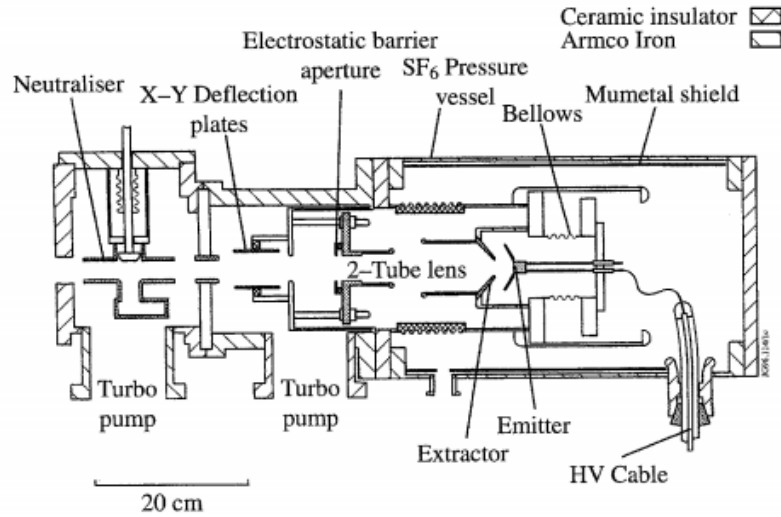


Figure 4.1: The improve version of the ASDEX gun, source: [6]

The Li-beam diagnostic was equipped in 2014 with a 32 channel APD (advance photo-diode) detector system. Most of the detectors collect light from optical channels looking onto the center of the Li-beam, but there are also some channels looking to the flanks. The central channels are used for the calculation of the fluctuation relative amplitude, while correlation analysis between channels looking at the same major radius but different poloidal location reveal the poloidal flow velocity. This device gets a voltage signal in every one of their channels, and using the IPP model it returns a random data signal.

In order to distinguish the lithium photons from the ones coming from the background radiation, the diagnostic has an on-off period. The difference can be seen in the figure 4.2.

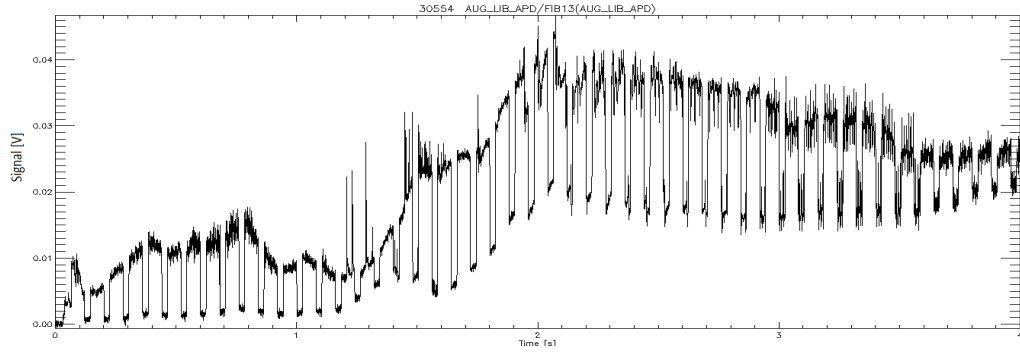


Figure 4.2: raw signal obtained from ASDEX Up

4.3 Experiment setup

The experiments we analyzed are a series of experiments performed in 2014 with very similar characteristics. The plasma was heated until 150 million °C in two phases. In second 2,1 ($t = 2.1s$) of the discharge the heating current starts pulsing until it gets continue at second 2,5 ($t = 2.5s$) and the second phase doubles the heating power from $t = 2.6s$ to $t = 2.7s$. This procedure is carried out twice in each experiment, or shot, as we can see in figure 4.3 with different plasma densities. Those density profiles were studied in [25].

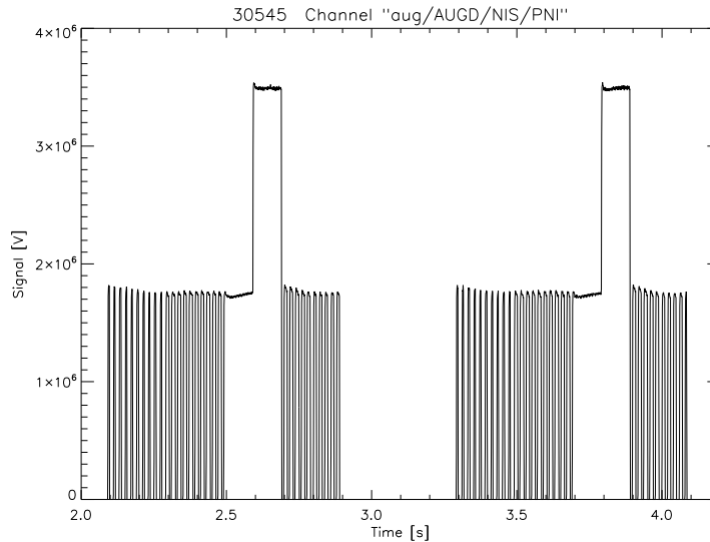


Figure 4.3: Plasma heating current of discharge 30545

4.3.1 Selection of time intervals

In order to compare the results and get more information of the resulting plots we have cut the signal of every discharge in different time ranges according to the different phases of the plasma discharge, this distinction allow us to analyze the behavior of the plasma in different conditions. We studied the low confinement mode (L-mode), the intermediate phase (separated in two time ranges because the behavior was also different) and high confinement mode (H-mode). We also considered interesting to analyze separately in H-mode time intervals containing ELMs (edge localised mode) and time intervals between ELMs as can be seen in figure 3.3 and 3.4. Also in all of this time ranges he separated the signal when the li-beam was on and when it was off. This allow us to distinguish and separate the signal from the background.

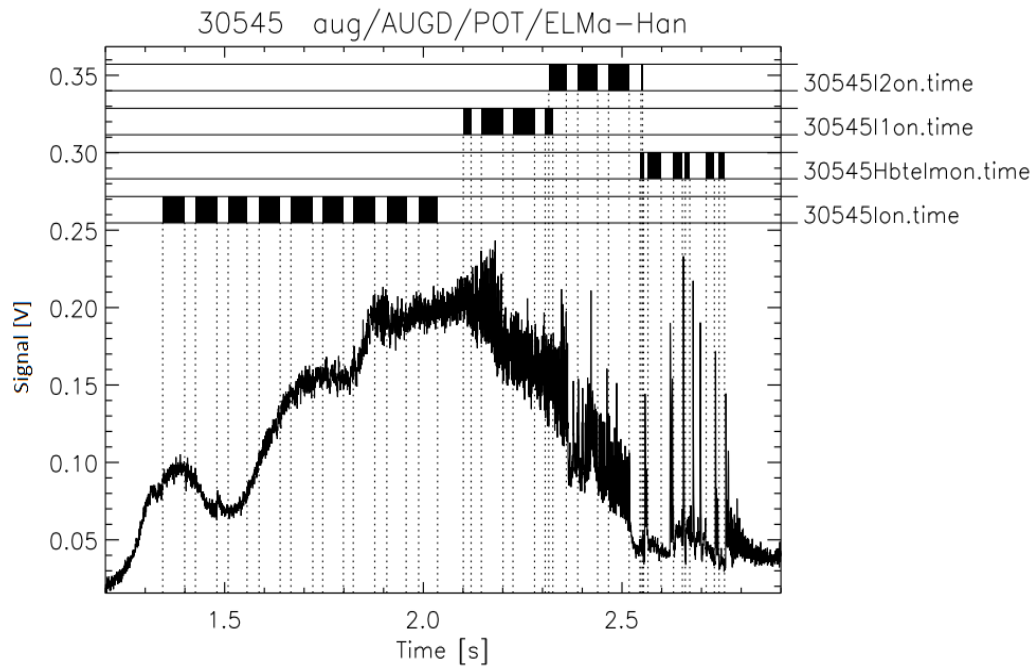


Figure 4.4: The selection of the time intervals seen on the raw signal from the divertor, density 1.

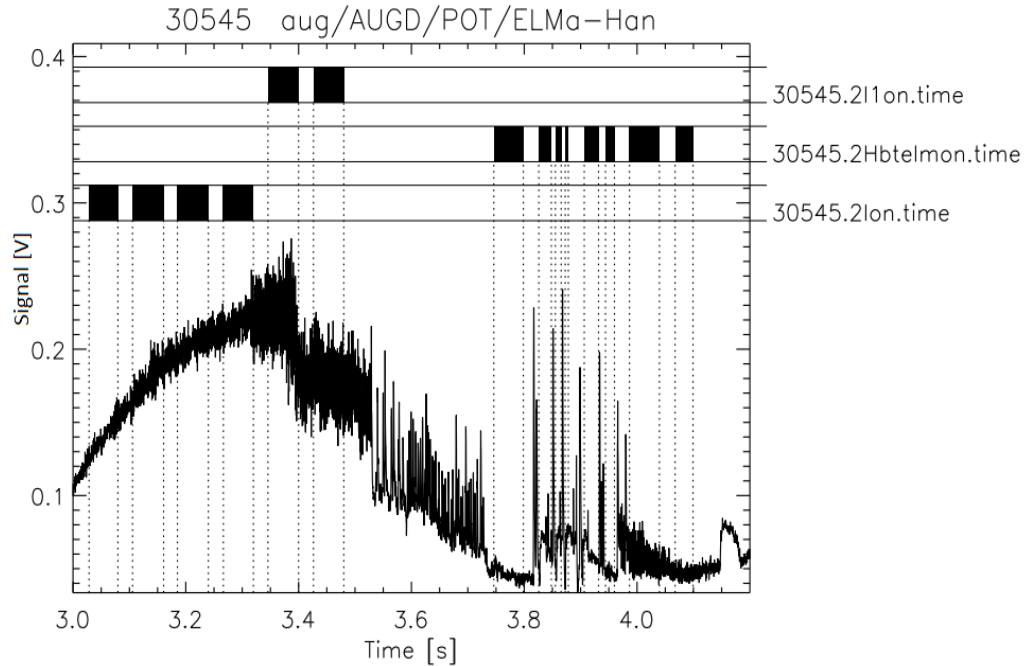


Figure 4.5: The selection of the time intervals seen on the raw signal from the divertor, density 2.

4.4 Data treatment

The data gathered during the experiment comes from stochastic process which is the excitation decay of the lithium atoms shoot into the plasma. That is why we need to choose how important is every part of this signal. And the way we decomposed that signal was through the Fourier transform.

4.4.1 Fourier transform

The Fourier transform is a mathematical mechanism that divides a function of time into the frequencies that make it up. The Fourier transform absolute value means the amount of that frequency present in the initial function, and whose complex argument is the phase offset of the basic sinusoid in that frequency.

The Fourier transform is also called the frequency domain representation of the original signal. The Fourier transform is not bounded to functions of time, but in order to have a unique language, the domain of the original function is

normally referred to as the time domain [26].

Linear operations performed in one domain (time or frequency) have corresponding operations in the other domain. As an example, the differentiation in the time domain has a correspondence to multiplication by the frequency, this way some differential equations are easier to analyze in the frequency domain.

Concretely, this means that any linear time-invariant system, such as a filter applied to a signal, can be expressed in a simply way as an operation on frequencies. After performing the desired operations, transformation of the result can be made back to the time domain [27].

Functions that are defined in the time domain have Fourier transforms that are spread out across the frequency domain and viceversa, a phenomenon known as the uncertainty principle. The critical case for this principle is the Gaussian function, of substantial importance in probability theory and statistics as well as in the study of physical phenomena exhibiting normal distribution (e.g., diffusion).

The Fourier transform of a Gaussian function is another Gaussian function. Joseph Fourier introduced the transform in his study of heat transfer, where Gaussian functions appear as solutions of the heat equation [28].

There are several common conventions for defining the Fourier transform \hat{f} of an integrable function $f : \mathbb{R} \rightarrow \mathbb{C}$.

This work will use the following definition:

$$F(\omega) = \int_{-\infty}^{\infty} f(t)e^{-i\omega t} dt \quad (4.1)$$

4.4.2 Calculating the power spectra

For the calculation of the power spectra first the signal was transferred to the frecuencial domain with the fourier transform:

$$F(\omega) = \int_{-\infty}^{\infty} f(t)e^{-i\omega t} dt \quad (4.2)$$

Power spectrum is calculated as the convolution of the Fourier transform and the conjugate of the Fourier transform. This operation cancels all the imaginary part of the Fourier transform, or offset, and leave only the absolute value of the signal intensity

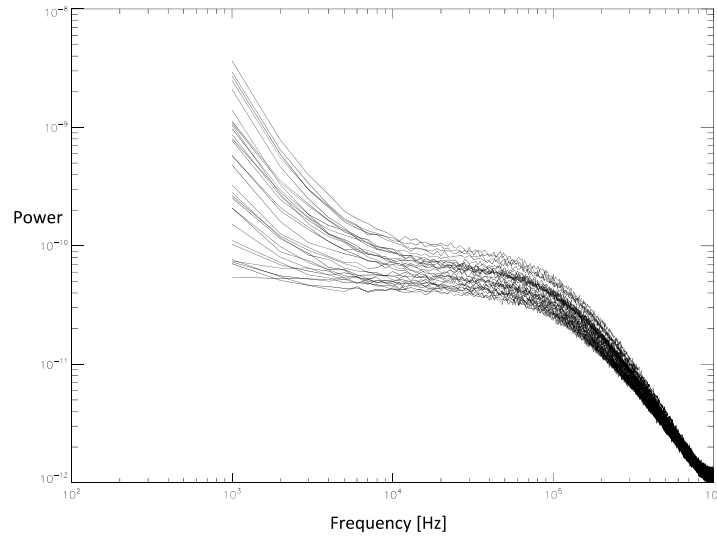


Figure 4.6: Power spectra of the signals from all the channels on shoot 30548

4.4.3 Estimation of noise level

Due to nature of the material used obtaining the signals there will be presence of noise coming from the optics, the amplifier and other electric devices. So the complete signal will be the addition of the detection plus the noise:

$$N_e(t) = I(t) + noise \quad (4.3)$$

The detector and photon statistical noise was calculated and subtracted from the spectra by considering that between 150 and 450 kHz only noise was present and noise spectra are flat in the whole frequency range of interest.

It is important to know where this noise is coming from. In our case, most of the noise is coming from the signal amplifier. We see that thanks to the analysis of the Fourier transform. The estimation of the noise level we calculated the power spectra of the whole signal. We know the shape of the power spectra of the noise [29]. As shown in figure 4.6.

From the noise corrected spectra the power was integrated between frequencies $1.5 \cdot 10^4$ and $5 \cdot 10^4$ Hz.

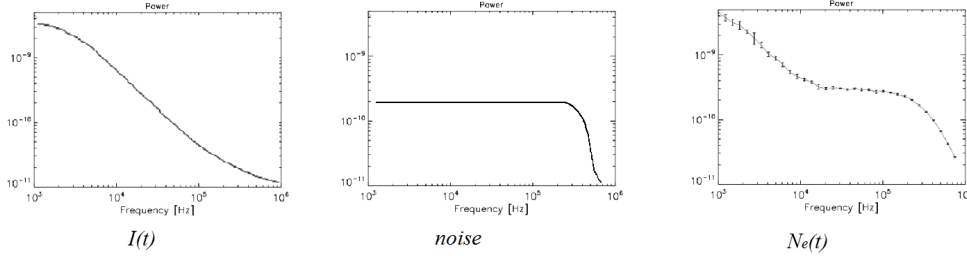


Figure 4.7: Power spectra of the intended signal, noise and the obtained signal

4.4.4 Calculation of fluctuation amplitude

In order to obtain useful information of the data we gathered, we looked for the fluctuation amplitude of the signal. From the resulting integrated power P the relative fluctuation amplitude was calculated as the

$$r = \frac{\sqrt{2P}}{\langle S \rangle} \quad (4.4)$$

where $\langle S \rangle$ is the mean signal in the time interval of interest. For comparison the fluctuation power in the beam-off time interval or background was also calculated and normalised by the mean signal in the beam-on period. Using these results we can see whether the fluctuation is due to the beam light or background.

4.4.5 Calculation of correlations an flow velocity

We used the convolution of the signal in two consecutive periods

Making use of the poloidal offset of the optical fibers, the poloidal velocity was calculated and plotted. For this signals were selected where at least two fibres look on the beam at the same radius but poloidally offset. (There are radii where there are also 3 such fibres.) The maximum time lag of the crosscorrelation function between the signal measured in the central fibres and poloidally offset one is calculated. From this the poloidal velocity is calculated and averaged for one major radius. The resulting plow velocity profile is plotted.

4.5 Algorithm

In this section, the logic of the used algorithm is explained. To see the full code, see Appendix A.

The algorithm used to analyze the relative fluctuation and flow velocity was developed with an IDL language and environment. The program has some different parts, explained in the following lines.

Firstly, some values have to be set for every shot we want to analyze. Therefore, we initialize the parameters of the frequency range, and the parameters used to filter the noise. Such parameters have been deduced from a primary analysis of the power spectrum (see figure 4.6).

Later, we calculate how many active channels had this discharge to be able to go over all of them.

For each channel, the data is transformed by the Fourier transform and we obtain, through a simple operation, the power spectrum. This sequence is repeated with the beam off signal. The obtained power spectra is integrated in the range set on the parameters.

It is here where the noise is filtered in order to get clearer results.

The next step of the code is to calculate the fluctuation amplitude for the signal and the background and we normalize both fluctuation amplitudes by the signal mean.

The flow velocity is calculated using the correlation function of the fluctuation of two channels, a central one and another poloidally offset. A time lag is obtained from this process, and using a fibre map we calculate the flow velocity. This process is repeated for every central channel with a correspondence with another poloidally offset.

The final step is to plot the relative fluctuation amplitude and the flow velocity.

Chapter 5

Results and discussion

In this chapter, the results of the experiment are presented. In order to have some statistical correct results, the same setup was repeated in several discharges. For every time range selected we generated a post script file with two plots. But a lot of the showed incongruous results and we decided to keep most of them out of the report.

5.1 Fluctuation amplitude and flow velocity profiles

In each plot the filled circles indicate beam-on times while the open rectangles beam off (i.e. background) periods. The dot line in figure 5.1 at $R = 2.125m$ represents the point where separatrix meets the li-beam, there's where our diagnosis system detects the beginning of the SOL.

The plots from figure 5.2 to figure 5.10 show the evolution in time of the SOL turbulence behavior in shot 30545. This shot is the one that gave us best results. Even if its true that all shots have similar setups the results had appear to be different from each other.

Looking to the resulting plots we can observe the following behavior:

- The value of the relative fluctuation rises greatly on the outer side of the separatrix, or what means the same, in the SOL. The fluctuation reaches the 60% in most cases and the 80% exceptionally.
- We have seen a change in the behavior of the SOL turbulence during the transition from L mode to H mode but not always in the same direction.

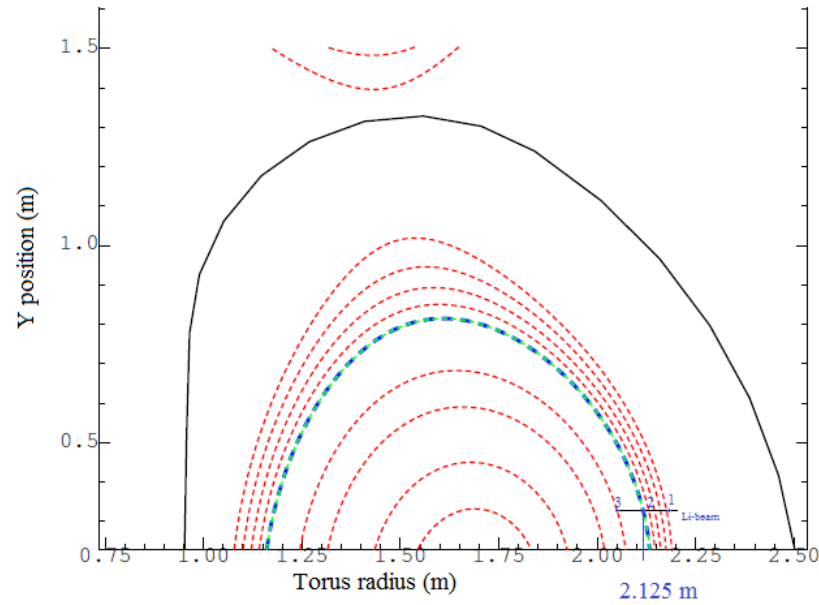


Figure 5.1: Plasma profile during 30545 experiment. Source: IPP

- Analyzing figure 5.6, figure 5.17 and figure 5.22 we see that during the ELMs the fluctuation is higher also inside the confined plasma.
- The results seen in figure 5.11, figure 5.12 and figure 5.13 are examples of what we considered bad plots with incongruous results, where the background fluctuation, normalized by the mean signal of the beam-on period, is higher in many points than the signal fluctuation
- It is important to point out that we have observed a curious behavior on the turbulence transport when we arrive to the H mode. The turbulence go backwards back to the plasma. This phenomena happens on both sides of the separatrix but it appears to be more important on the outer side.

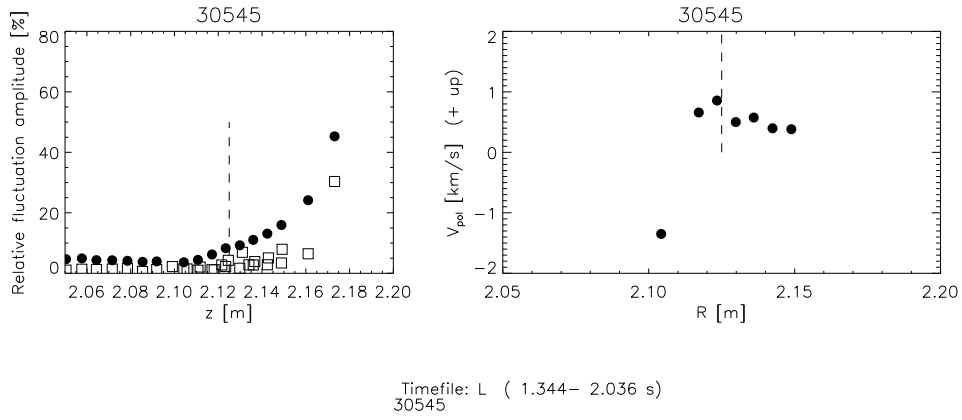


Figure 5.2: Relative fluctuation amplitude and poloidal velocity in shot 30545 during L mode with density 1.

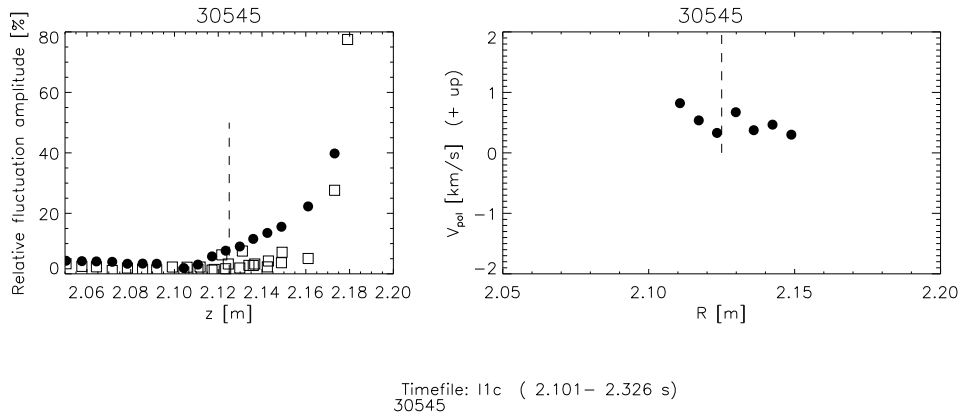


Figure 5.3: Relative fluctuation amplitude and poloidal velocity in shot 30545 during the first part of the intermediate phase with density 1.

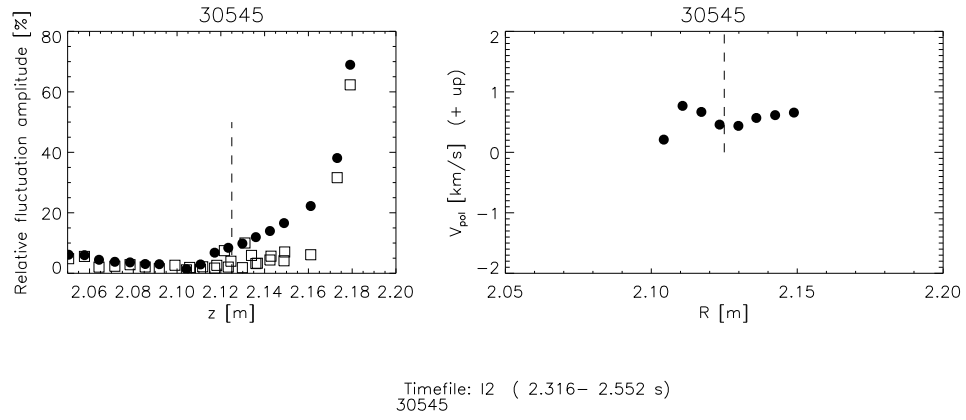


Figure 5.4: Relative fluctuation amplitude and poloidal velocity in shot 30545 during the second part of the intermediate phase with density 1.

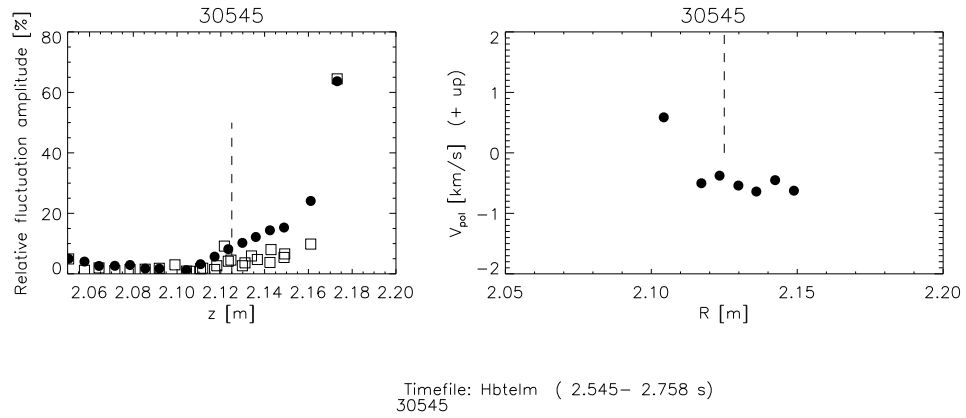


Figure 5.5: Relative fluctuation amplitude and poloidal velocity in shot 30545 during H mode taking the data in between ELMs with density 1.

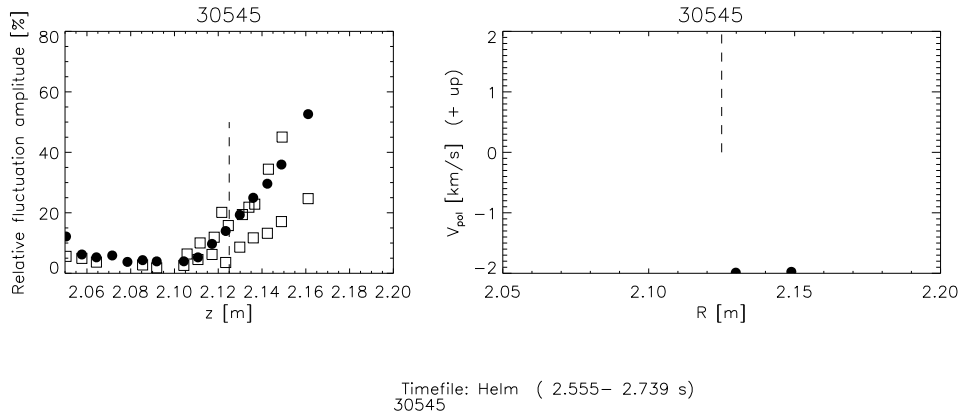


Figure 5.6: Relative fluctuation amplitude and poloidal velocity in shot 30545 during H mode during the ELMs, with density 1.

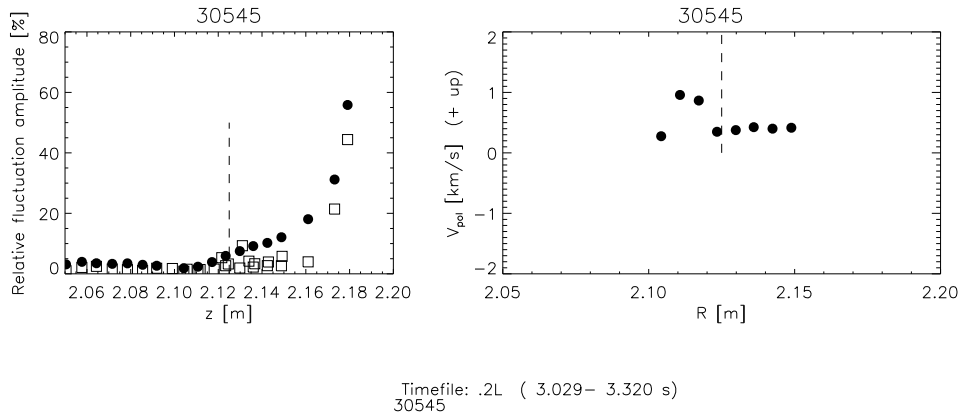


Figure 5.7: Relative fluctuation amplitude and poloidal velocity in shot 30545 during the L mode with density 2.

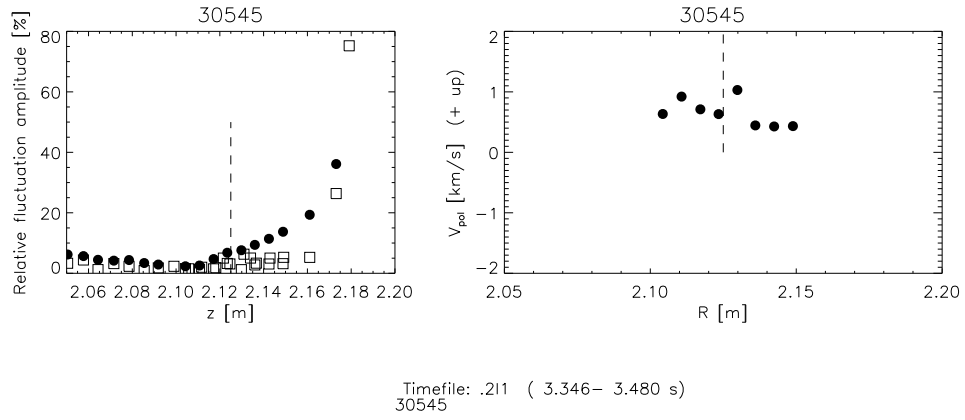


Figure 5.8: Relative fluctuation amplitude and poloidal velocity in shot 30545 during the first part of the intermediate phase with density 2.

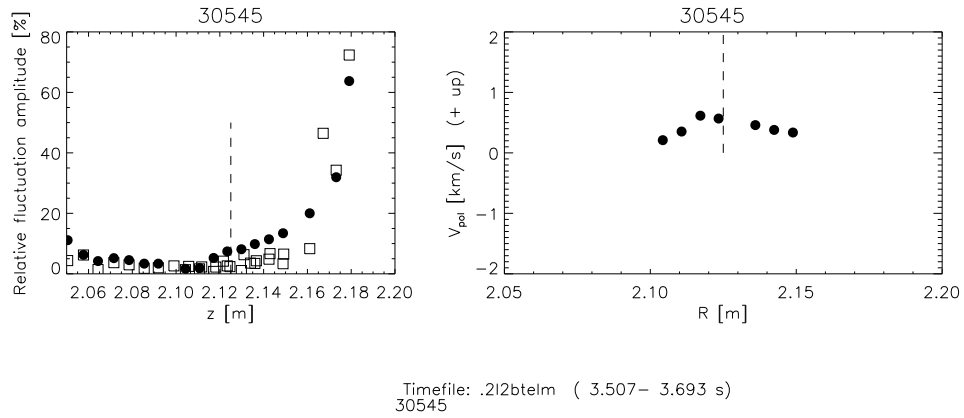


Figure 5.9: Relative fluctuation amplitude and poloidal velocity in shot 30545 during the second part of the intermediate phase with density 2.

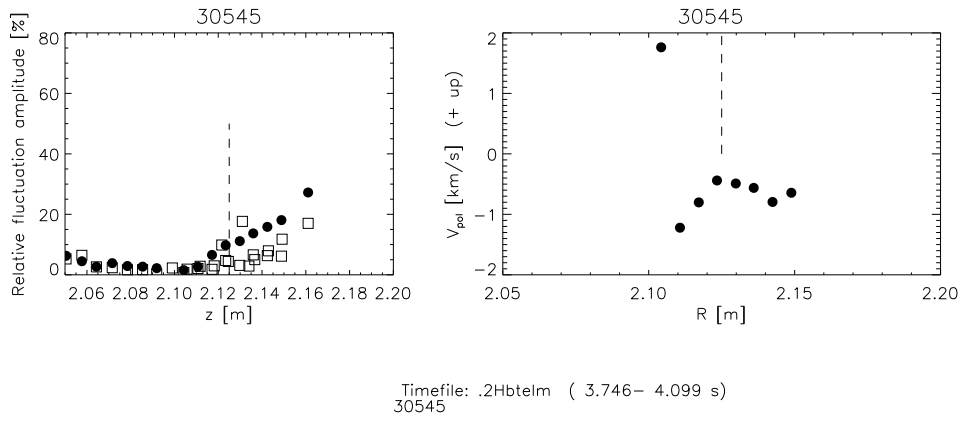


Figure 5.10: Relative fluctuation amplitude and poloidal velocity in shot 30545 during the H mode, taking the data between the ELMs. With density 2.

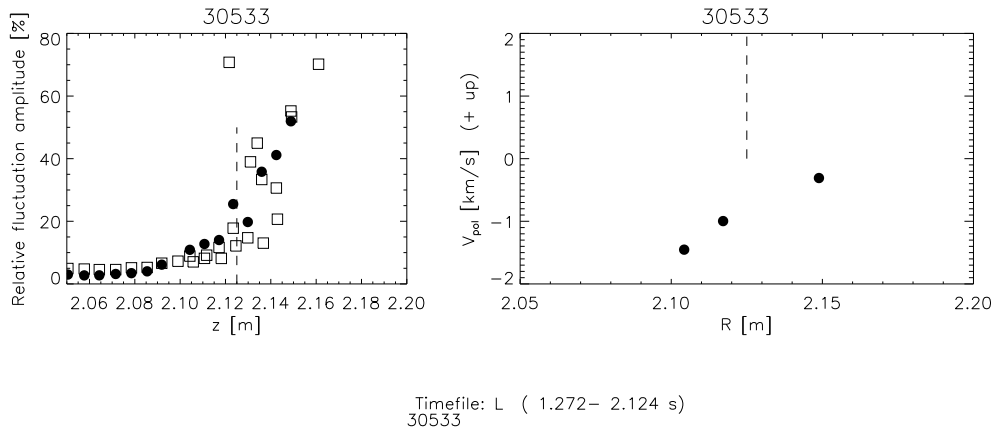


Figure 5.11: Relative fluctuation amplitude and poloidal velocity in shot 30533 during L mode with density 1

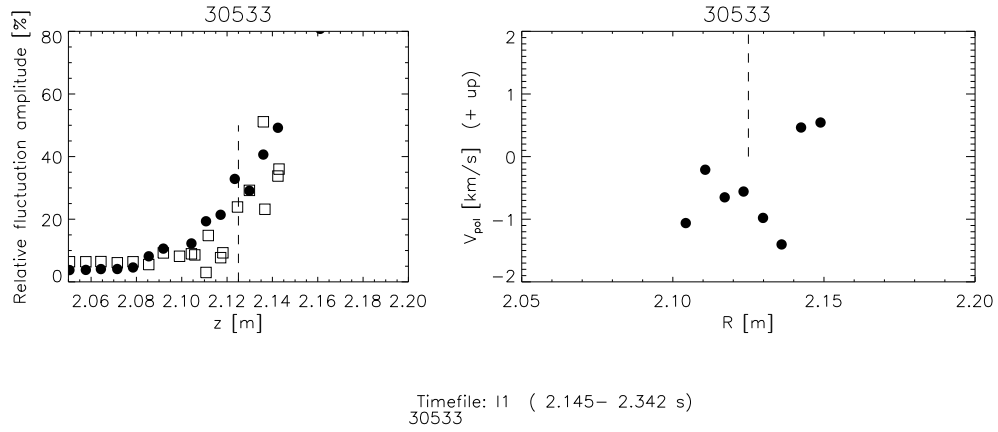


Figure 5.12: Relative fluctuation amplitude and poloidal velocity in shot 30533 during the intermediate phase with density 1

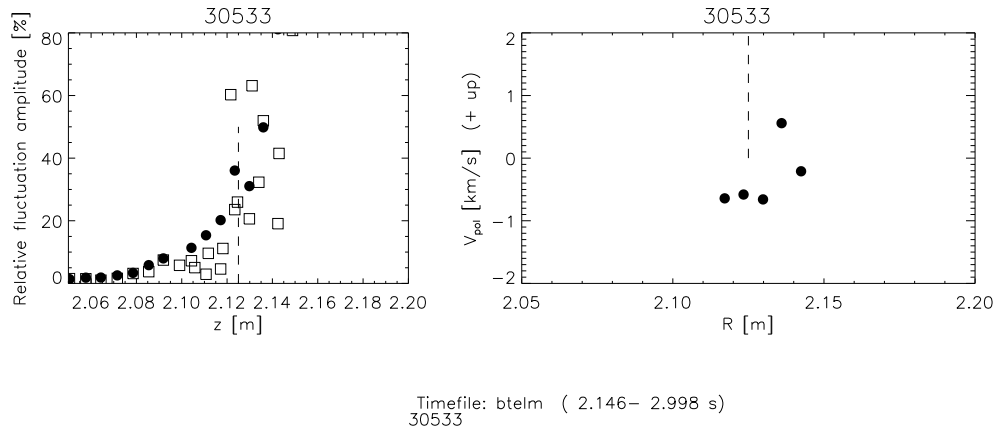


Figure 5.13: Relative fluctuation amplitude and poloidal velocity in shot 30533 during H mode and density 1.

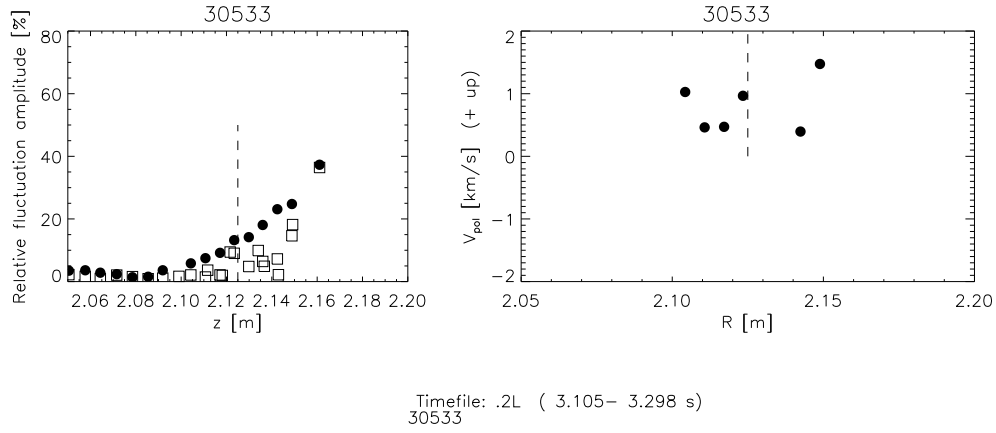


Figure 5.14: Relative fluctuation amplitude and poloidal velocity in shot 30533 during the L mode with density 2.

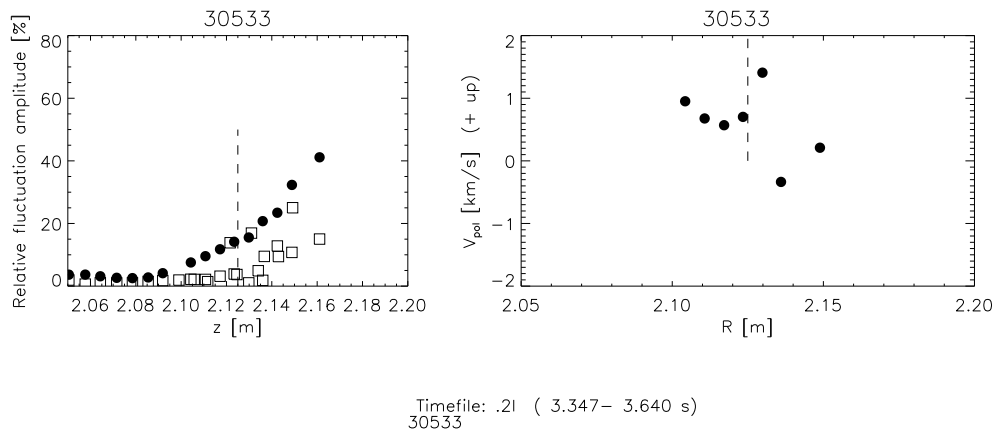


Figure 5.15: Relative fluctuation amplitude and poloidal velocity in shot 30533 during the intermediate phase with density 2.

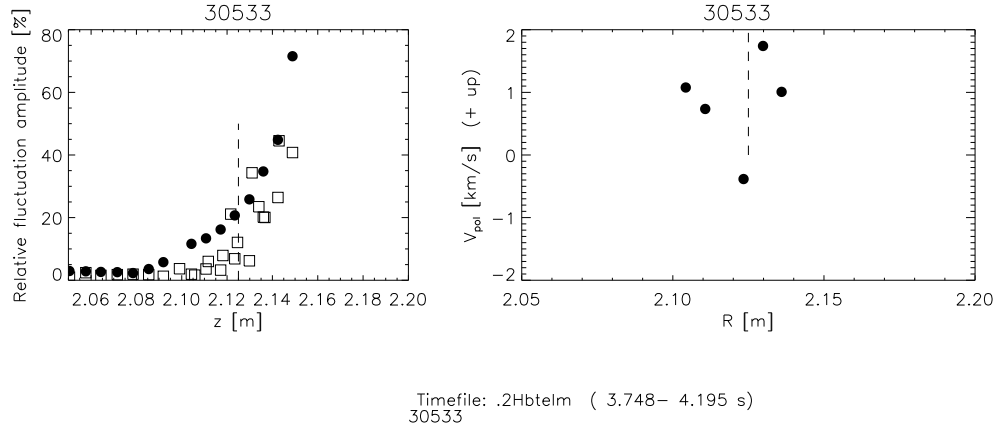


Figure 5.16: Relative fluctuation amplitude and poloidal velocity in shot 30533 during the H mode and taking only the data between the ELMs, with density 2.

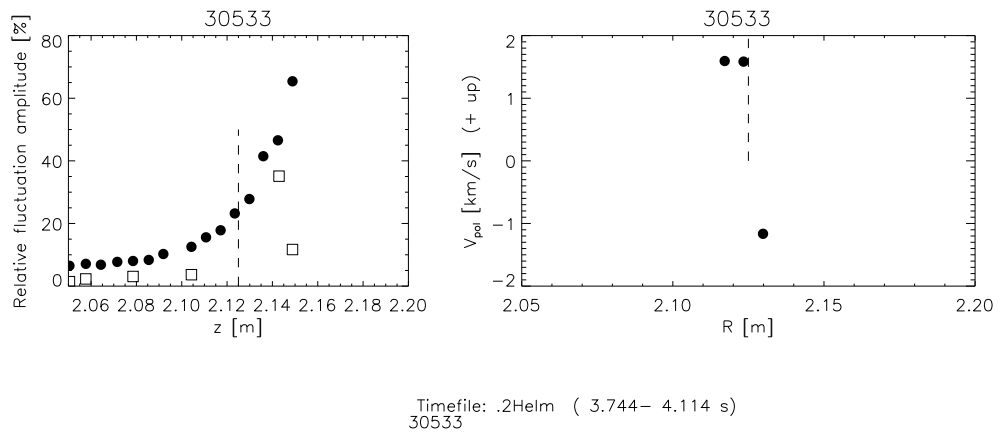


Figure 5.17: Relative fluctuation amplitude and poloidal velocity in shot 30533 during the H mode and taking only the data during the ELMs, with density 2.

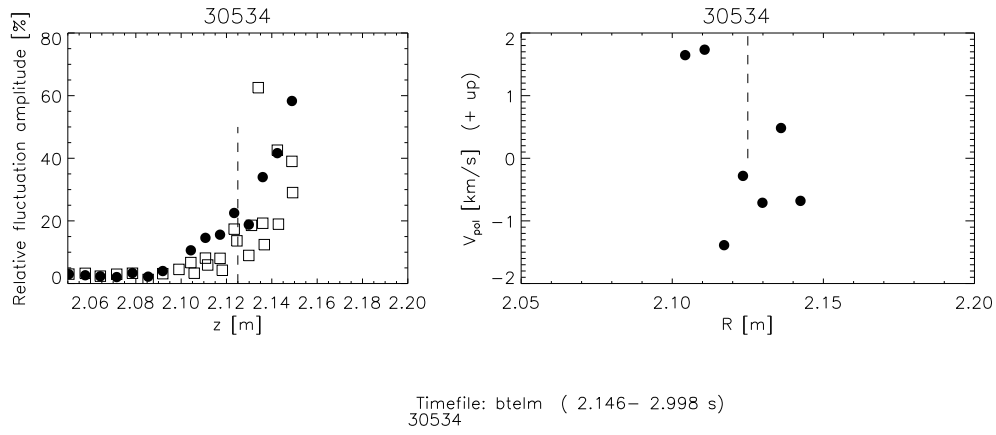


Figure 5.18: Relative fluctuation amplitude and poloidal velocity in shot 30534 during H mode between ELMs and density 1.

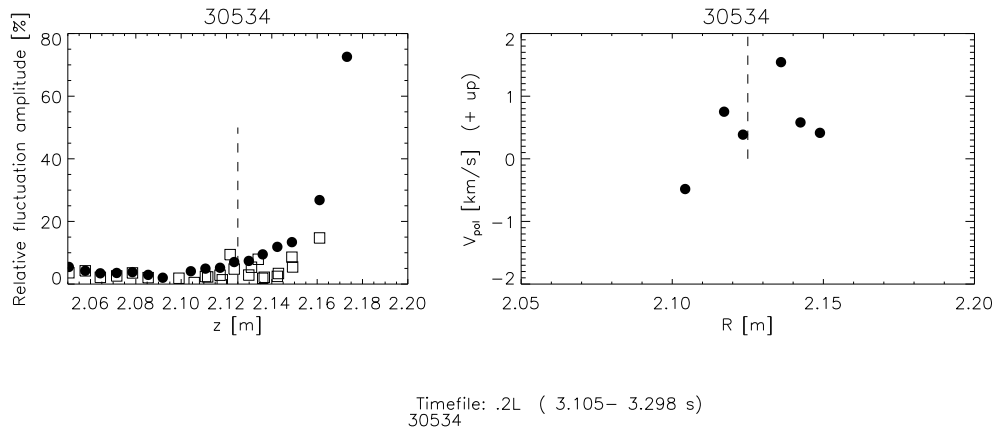


Figure 5.19: Relative fluctuation amplitude and poloidal velocity in shot 30534 during the L mode with density 2.

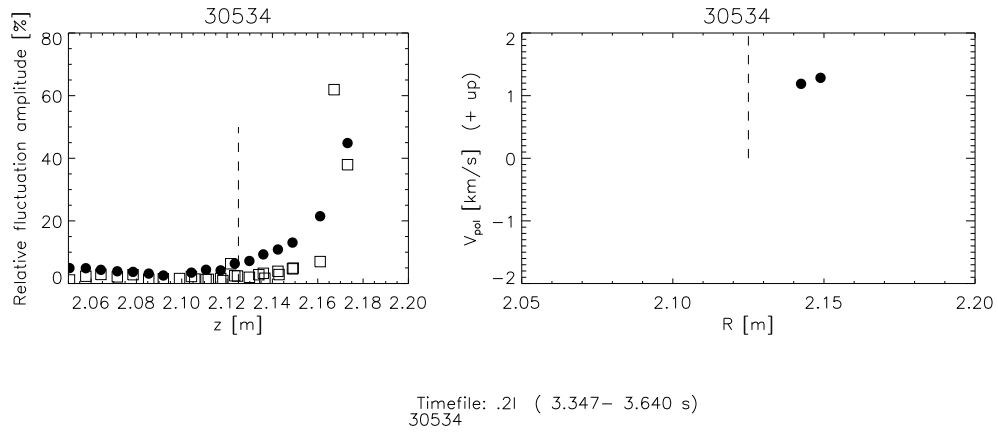


Figure 5.20: Relative fluctuation amplitude and poloidal velocity in shot 30534 during the intermediate phase with density 2.

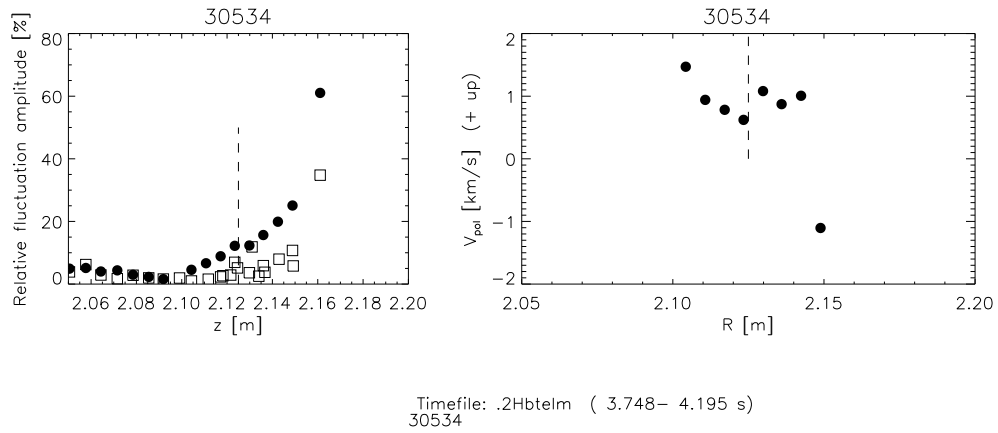


Figure 5.21: Relative fluctuation amplitude and poloidal velocity in shot 30534 during the H mode and taking only the data between the ELMs, with density 2.

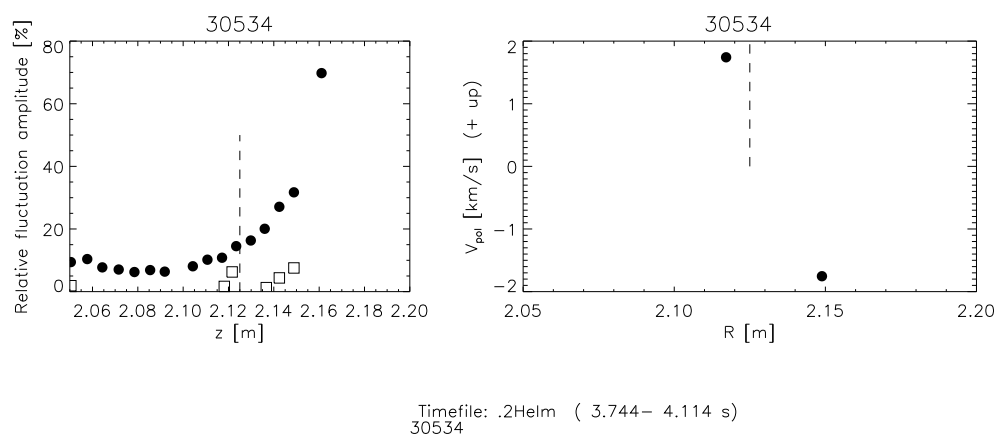


Figure 5.22: Relative fluctuation amplitude and poloidal velocity in shot 30534 during the H mode and taking only the data during the ELMs, with density 2.

Chapter 6

Ecological and economic analysis

The cost on this thesis are basically human power, and the diagnosis material and the cost of the reactor.

6.1 Budget

To elaborate this thesis, as it is a theoretical research, the main cost has been the human resources dedication. In addition, some expenses have been done in material resources, but in a minor scale, as detailed in the following subsections.

6.1.1 Human resources

The author of this thesis has dedicated a total of 600 hours with a cost per hour of 25 €. The director had dedicated 100h and the local tutor 20 hours, being their cost per hour 70 €. See table 6.1

Human resources	Unitary price (€/h)	Time (h)	Total (€)
Author of the project costs	25	600	15.000,00 €
Director of the project costs	70	100	7.000,00 €
Local tutor of the project cost	70	20	1.400,00 €
TOTAL before taxes	-	-	23.400,00 €
Taxes (VAT 21%)	-	-	4.914 €
TOTAL	-	-	28.314 €

Table 6.1: Human resources used on the creation of this thesis and their economic cost

6.1.2 Material resources

The fulfilment of this project required the use of different software, two for obtaining the data (an SSh client, bitvise) and treating the data (IDL programing environment). It was obviously necessary a computer, from which we consider the amortization of the initial cost and the expected lifespan. We will not consider any other software because for the writing and other minor needs we used free license programs.

Another expense was printing the necessary literature to read and analyze such as papers, articles, and abstracts from other thesis. It is estimated that around 300 copies have been printed, in recycled double-sided paper.

The expenses related to bibliography have been null. This is because different reasons: either the resources were consulted in the library, or the books were lent by the tutor of this thesis and other consulted people.

Finally as a material expense for this project, the deliver of the thesis needed printing and binding of three copies to deliver to the university and the CDs we burned with the data.

All these calculations can be seen in table 6.2

Table 6.2: Material resources used on the creation of this thesis and their economic impact

	Unitary cost (€/unity)	Unities	Total (€)
IDL License	600	1	600
Software license	800	1	800
Amortization computer		1	150
Project bibliography printings	0.035	100 x 2	7
Bibliography	0	-	0
Printing and binding of the thesis	15	3	45
PFC CDs	3	5	15
Total before taxes			1.617 €
Taxes - VAT 21%			339,57 €
TOTAL			1.956,57 €

6.1.3 Energetic resources

Related to energetic resources, it is estimated that in 600 hours of dedication to the project have been using the computer and this has caused the corresponding electricity consumption. In the same line, some artificial illumination has been needed during certain times of the elaboration, assuming around 250 hours of light with energy consumption associated.

6.2 Ecological analysis

The main resource used during the elaboration of this thesis has been a computer. The author uses a personal laptop, with an electrical adaptor of 60W, which is used to recharge the battery, and has approximately the same autonomy of time as the time used for recharging. This is to say, if the work time has been 600 hours with the computer, this computer has been connected to the electric grid for 300 h. This has caused a consumption of 18 kWh.

As mentioned before, the auxiliary consumption has been due to illumination: for this project, some artificial light has been needed, around 250 hours. Mainly, the table lamp of the author, which is driven by a low consumption bulb with a power of 13W, causing the consumption of 3,25 kWh.

According to the electric mix of the Spanish electrical system, the electrical consumption causes the emission to the atmosphere of 0,4 kg of CO_2 per kWh, causing this project to throw 8.5 kg of CO_2 due to electrical consumption. However, this project has been mainly performed at the authors home, which buys the electricity to a company that only sells "green" electricity, so the electrical consumption has not caused any harm to the environment.

Chapter 7

Conclusions

In this chapter the conclusions obtained after the discussion will be explained. First, the findings will be shown followed by the achievements of the goals raised in the introduction.

7.1 Findings

- The Li-beam diagnostic is capable of measuring SOL fluctuations in the plasma both in L and H mode. The fluctuation amplitude and their poloidal flow velocity can be determined.
- As the Lithium beam is non-perturbing diagnostic it can be used in all discharges unlike probes which are limited to certain times and perturb the plasma.
- The fluctuation amplitude and the measurement sensitivity drops inside the separatrix, therefore with the present optics it is not possible to measure plasma turbulence inside the separatrix.
- The plots obtained show a great resemblance between the relative fluctuation of the signal and the background. Both depend on the position in the main radius and the turbulence grows as it separates from the separatrix.
- During the ELMs the fluctuation amplitude is higher and the background light also has much higher amplitude. This inhibits measuring the poloidal flow velocity of plasma turbulence during ELMs.

- The fluctuation amplitude between the ELMs in H-mode is very similar to the L-mode case. This indicates that the SOL turbulence is decoupled from the plasma edge turbulence.
- Regarding the poloidal velocity it has been observed repeatedly a reverse in the poloidal direction of the plasma turbulence once they reach the separatrix. This phenomenon happens strongly in H mode.

7.2 Goals achievement

We consider the following goals announced in 2.3 achieved:

- A program to calculate the dimension of the turbulence was designed. We could calculate the magnitude and the transport inside and outside the SOL.
- We have seen a little more about how those turbulence behave inside the SOL during the H mode, the reversal flow was something we didn't expect.

We also consider some of the questions asked at the beginning answered:

- We have shown a possible design for a filter program that could partially show the behavior of the turbulence
- The dimension of the turbulence was also answered setting a dependence between the radial position and the magnitude of the turbulence

7.3 Future work

Even if the reversal flow velocity appears to be a robust effect, it should be compared with other measurements of the same shot and also with other shots. This project did not achieve strong conclusions about the turbulence, we don't exactly know how it affects the transport.

Bibliography

- [1] Alan Boyle. Nuclear fusion gets boost from private-sector startups. *ScienceNews*, 189(3):18, 2016.
- [2] Euro fusion. <https://www.euro-fusion.org/downloads/hydrogen-deuterium-tritium/>, 2011. [Online; accessed 01-August-2016].
- [3] D Petkow, RA Gabrielli, G Herdrich, R Laufer, and H-P Röser. Generalized lawson criterion for magnetic fusion applications in space. *Fusion Engineering and Design*, 87(1):30–38, 2012.
- [4] Battery and energy technologies. http://www.mpoweruk.com/nuclear_practice.htm, 2015.
- [5] A new fusion collaboration for mit: Wendelstein 7-x begins operation. mit. <https://www.psfc.mit.edu/>, 2015.
- [6] G. Kocsis J. Schweinzer K. McCormick, S. Fiedler and and S. Zoletnik. Edge density measurements with a fast li beam probe in tokamak and stellarator experiments. *Fusion Engineering and Design*, 34:125–134, 1997.
- [7] International energy agency. <http://www.iea.org/newsroomandevents/news/2013/June/name,38548,en.html>, 2013. [Online; accessed 19-July-2016].
- [8] IEA. *Resources to Reserves 2013*. International Energy Agency, 2013.
- [9] M. M. Hoogwijk B. J. M. de Vries, D. P. van Vuuren. Renewable energy sources: Their global potential for the first-half of the 21st century at a global level: An integrated approach. *Energy Policy*, 2007.

- [10] R. Moreno Salinas. *Advanced techniques of disruption prediction, application to JET and extrapolation to ITER*. PhD thesis, Universidad Nacional de Educaci' on a Distancia, 2015.
- [11] A.S. Eddington. *The Internal Constitution of the Stars*. 1926.
- [12] Irvin Langmuir Lewi Tonks. *Oscillations in ionized gases*. 1929.
- [13] Mitsuru Kikuchi. *Frontiers in fusion research: physics and fusion*. Springer Science & Business Media, 2011.
- [14] Garry McCracken and Peter Stott. *Fusion: the Energy of the Universe*. Academic Press, 2012.
- [15] H Bolt, V Barabash, W Krauss, J Linke, R Neu, S Suzuki, N Yoshida, and ASDEX Upgrade Team. Materials for the plasma-facing components of fusion reactors. *Journal of Nuclear Materials*, 329–333, Part A:66 – 73, 2004. Proceedings of the 11th International Conference on Fusion Reactor Materials (ICFRM-11).
- [16] C.M. Braams and P.E. Scott. *Nuclear Fusion. Hald a century of magnetic confinement fusion research*. IOP, 2002.
- [17] John N Bahcall, Lowell S Brown, Andrei Gruzinov, and RF Sawyer. The salpeter plasma correction for solar fusion reactions. *Astronomy & Astrophysics*, 383(1):291–295, 2002.
- [18] John D Lawson. Some criteria for a power producing thermonuclear reactor. *Proceedings of the Physical Society. Section B*, 70(1):6, 1957.
- [19] G. Petravich G. Anda and S. Bató S. Zoletnik. Li-beam developments for high-energy plasma diagnostics. *Operations ResearchFusion Engineering and Design*, 74:715–719, 2005.
- [20] A. Czopf D. Réfy, E. Wolfrum S. Zoletnik, and F. Laggner G. Birkenmeier. Asdex li-bes apdcam tests. *ASDEX APD test report*, 31 March 2014.
- [21] Ian H Hutchinson. Principles of plasma diagnostics. *Plasma Physics and Controlled Fusion*, 44(12):2603, 2002.

- [22] G Fuchert, G Birkenmeier, D Carralero, T Lunt, P Manz, H W Müller, B Nold, M Ramisch, V Rohde, and U Stroth. Blob properties in l- and h-mode from gas-puff imaging in asdex upgrade. *Plasma Physics and Controlled Fusion*, 56(12), 2014.
- [23] E Hintz and B Schweer. Plasma edge diagnostics by atomic beam supported emission spectroscopy-status and perspectives. *Plasma Physics and Controlled Fusion*, 37(11A):A87, 1995.
- [24] J. Schweinzer. , et al. Identification of plasma-edge-related operational regime boundaries and the effect of edge instability on confinement in asdex upgrade. *Plasma Physics and Controlled Fusion*, 37(11A):A87, 1995.
- [25] Sándor Zoletnik Carlos Silva, et al. Internal report wigner status may 2014.
- [26] Salomon Bochner and Komaravolu Chandrasekharan. *Fourier Transforms.(AM-19)*, volume 19. Princeton University Press, 2016.
- [27] David H Bailey and Paul N Swarztrauber. A fast method for the numerical evaluation of continuous fourier and laplace transforms. *SIAM Journal on Scientific Computing*, 15(5):1105–1110, 1994.
- [28] Javier Duoandikoetxea Zuazo. *Fourier analysis*, volume 29. American Mathematical Soc., 2001.
- [29] Julius S. Bendat and Allan G. Piersol. *Random Data: Analysis and Measurement Procedures*, chapter 5. John Wiley & Sons, Inc., 3rd edition, 2000.
- [30] T. Kobayash et al. Method for estimating the propagation direction of a coherent plasma structure using a one-dimensional diagnostic array. *Review of Scientific Instruments*, 85:083507, 2014.
- [31] M. Anton S. Zoletnik and S. Fiedler et al. M. Endler. Density fluctuation phenomena in the scrape-off layer and edge plasma of the wendelstein 7-as stellarator. *Phys. Plasmas*, 6:4239, 1999.

Appendices

Appendix A

Used code

A.1 Main code

```
pro show_fluc_vpol, shot,f1=f1, f2=f2, csum=csum, m=m, s=s, f3=f3, f4=f4,
amp=amp, tamp=tamp, tfile=tfile, ramp=ramp, fibnames=fibnames, r=r,
savefile=savefile,nocalculate=nocalculate, timeback=timeback, sptrx=sptrx, thick=thick,
xrng=xrng
default,shot,30545
default,fres,1e3
default,f1,1.5e4
default,f2,4e4
default, f3, 1e3
default, f4, 10e3
default, sptrx, 2.125
default, tfile,'.2I1'
default,savefile,dir_f_name('tmp','test.sav')
default, timeback, [1.564,1.584]

xrng=[2.05,2.2]

if (not keyword_set(nocalculate)) then begin
get_active_fib, shot, input_fibrenames=names
fnames='FIB'+names
tamp =fltarr(n_elements(names))
```

```
tampback =fltarr(n_elements(names))
map = get_asdex_obs_params(shot)
```

```
    fibnames=fix(reform(map[*],0))
r=fltarr(n_elements(fibnames))
z=fltarr(n_elements(fibnames))

    tramp=fltarr(n_elements(fibnames))
trampback=fltarr(n_elements(fibnames))
fluc_correlation, shot,i2str(shot)+tfile+'on.time', ref=fnames [i-1],
outpower= p,mean_ref=md,outfscale=f, fres=fres,
noplot,silent,errormess=errormess
for i=1, n_elements(names) do begin
if (errormess ne "") then begin
print,errormess
return
endif
```

```
    fluc_correlation, shot,i2str(shot)+tfile+'off.time',
ref=fnames [i-1], outpower= back,
mean_ref=mdback,outfscale=f, fres=fres,noplot,silent,errormess=errormess
if (errormess ne "") then begin
print, errormess
return
endif
ind = where ((f ge f1) and (f lt f2))
sum = total (p[ind])
sumback=total(back[ind])
csum = sum*2*fres
csumback=sum*2*fres
m=mean (p[ind])
mback=mean(back[ind])
max(p)],title=fibnames[i-1]
s=fltarr(n_elements(f))+m
sback=fltarr(n_elements(f))+mback
```

```

ind2= where((f ge f3) and (f lt f4))
amp= sqrt(total(p[ind2]-s[ind2])*2*fres)
ampback= sqrt(total(back[ind2]-sback[ind2])*2*fres)
md=md-mdback
ramp=amp/md
rampback=ampback/md
tamp[i-1]=amp
tramp[i-1]=ramp
trampback[i-1]=rampback
afibs=fix(names[i-1])
i2=where(fibnames eq afibs)

```

```

r[i-1]=map[i2[0],1]
z[i-1]=map[i2[0],2]
endfor
save,tramp,tamp,r,shot,file=savefile
endif else begin
restore, savefile
endelse
show_vpol_aug_li,shot,timefile=i2str(shot)+
+tfile+'on.time',no_lcfs,noerase,nolegend
restore,'tmp/show_vpol_aug_li.sav'

```

```

timefile=i2str(shot)+tfile

```

```

ind1= where(z lt 0.31)
ind2= where(z gt 0.325)
ind3= where((z gt 0.31)and (z lt 0.325))
r1=r[ind1]
tramp1=tramp[ind1]
r2=r[ind2]
tramp2=tramp[ind2]
r3=r[ind3]

```

```

tramp3=tramp[ind3]
plotsymbol,0
plot,r3, tramp3*100,thick= 1.5,
pos=[0.1,0.6,0.4,0.9],yrange=[0,80],charthick=1.5,
psym=8,xthick=
2,xstyle=1,xtitle='z [m]', ythick=2, ytitle='Relative fluctuation
amplitude [%]',xrange=xrng,title=i2str(shot),ystyle=1
plotsymbol, 3
oplot,r, trampback*100, psym=8,thick=2
if (defined(sptrx)) then begin
oplot,[sptrx,sptrx],[0,50],linest=2
endif
deftitle = i2str(shot)+' '
if (defined(timerange)) then begin
deftitle=deftitle+'['+string(timerange[0],format='(F6.3)')+','+'
+string(timerange[1],format='(F6.3)')+'] s'
timerange_sep = timerange
endif
default,title,deftitle
plotsymbol,0
plot, r_list,v_pol1000,noerase,pos=[0.5,0.6,0.9,0.9],xtitle='R
m
',xrange=xrng,ytitle='V!Dpol!N [km/s] (+
up)',yrange=[-2,2],title=title,thick=thick,xthick=thick,ythick=thick,
psym=8,charsize=charsize,charthick=thick,symsize=symsize,ystyle=1
if (defined(sptrx)) then begin
oplot,[sptrx,sptrx],[0,50],linest=2
endif
xyouts, 0.5,0.5,string(timerange[0],format='(F6.3)')+','+'
format='(F6.3)')+'] s',/normal
d=loadncol(dir_f_name('Time',i2str(shot)+tfile+'on'+'.time'),2,/silent,
errormess=errormess)
tindex = ' Timefile: ' +tfile
if (errormess eq '') then begin
tindex = tindex+'

```

```
('+string(min(d),format='(F6.3)')+ '-' +string(max(d),format='(F6.3)')+ ' s')'  
endif  
xyouts, 0.4,0.45,tindex+'!C'+i2str(shot),/normal  
end
```